SUPPLEMENTAL MATERIAL

Downregulation of *FBXO2* is associated with Aβ aggregation, tau hyperphosphorylation and network impairment in human cortical neurons

Alicia González Díaz[1,2], Andrea Possenti[1,2], Gustavo Antonio Urrutia[1,2], Yuqi Bian[1,2], Shekhar Kedia[2,3], Dorothea Boeken[2,3], Christine M. Lim[1,2], Danilo Licastro[4], Benedetta Mannini[1,2], David Klenerman[2,3], Michele Vendruscolo[1,2,*]

[1]*Centre for Misfolding Diseases, University of Cambridge, CB2 1EW Cambridge, UK*
[2]*Yusuf Hamied Department of Chemistry, University of Cambridge, CB2 1EW Cambridge, UK*
[3]*UK Dementia Research Institute, University of Cambridge, Cambridge, CB2 0AH, UK*
[4]*AREA Science Park, Padriciano 99, 34149 Trieste, Italy*

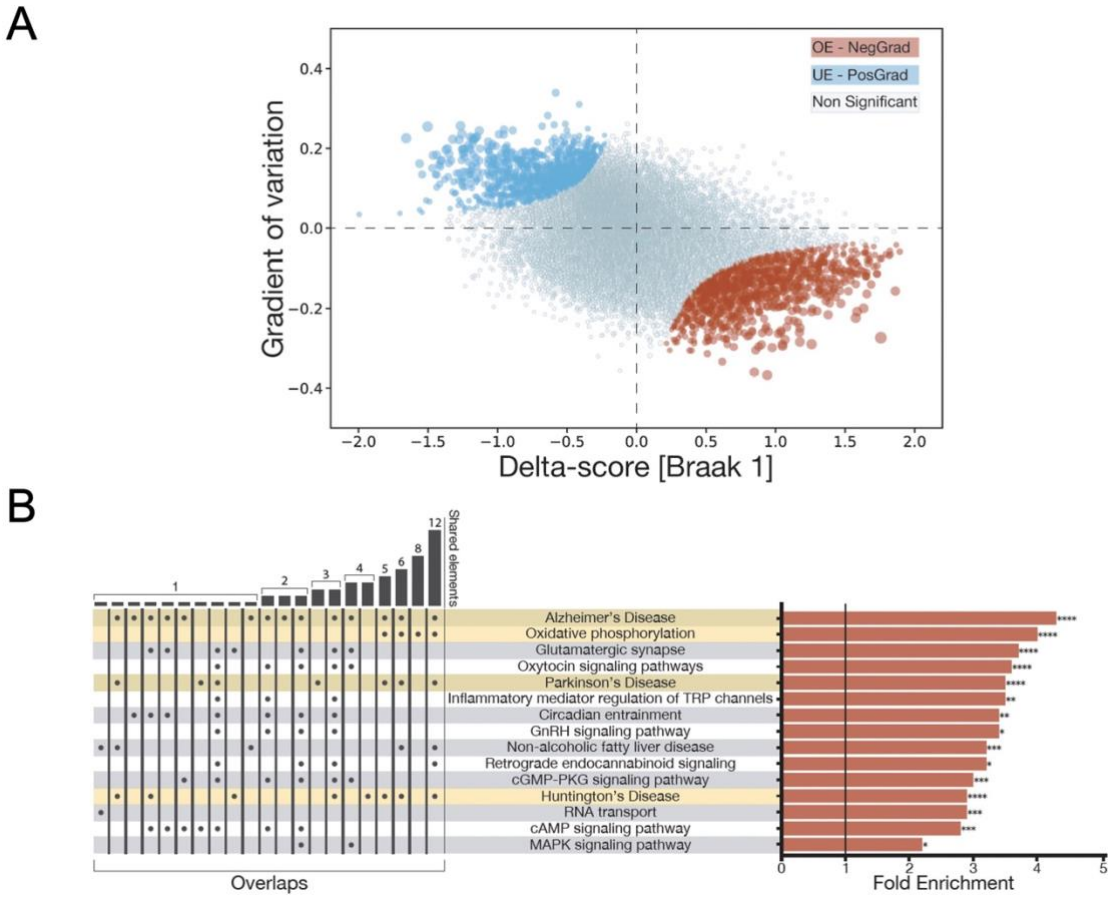

Figure S1. Identification of an initial set of guide genes with regional expression differences aligned with Braak staging. (**A**) Scatter plot of the genes median Δ scores in Braak I regions against their variation across the regions defining the staging. We identify 3 subsets of genes: over-expressed genes in Braak I with a negative gradient (OE - NegGrad, in red); under-expressed genes in Braak I with a positive gradient (UE - PosGrad, in light blue); non-significant genes (Non Significant), which do not show any particular pattern of variation. The size of the points is proportional to the vulnerability score Vg of a gene, with genes belonging to the tails scoring higher. (**B**) Fold enrichment of KEGG pathways in the OE - NegGrad tail of the Vg distribution. Pathways associated with neurodegenerative disorders are significantly enriched (yellow bars). On the left the overlap between each enriched pathway and the ones associated to neurodegeneration, showing a total of 60 genes represented in the enrichment. Significance was calculated with Fisher's exact test, with the transcriptome as a background, and corrected with a Bonferroni multiple hypothesis testing correction *p < 0.05, **p < 0.01, ***p < 0.001, ****p < 0.0001.

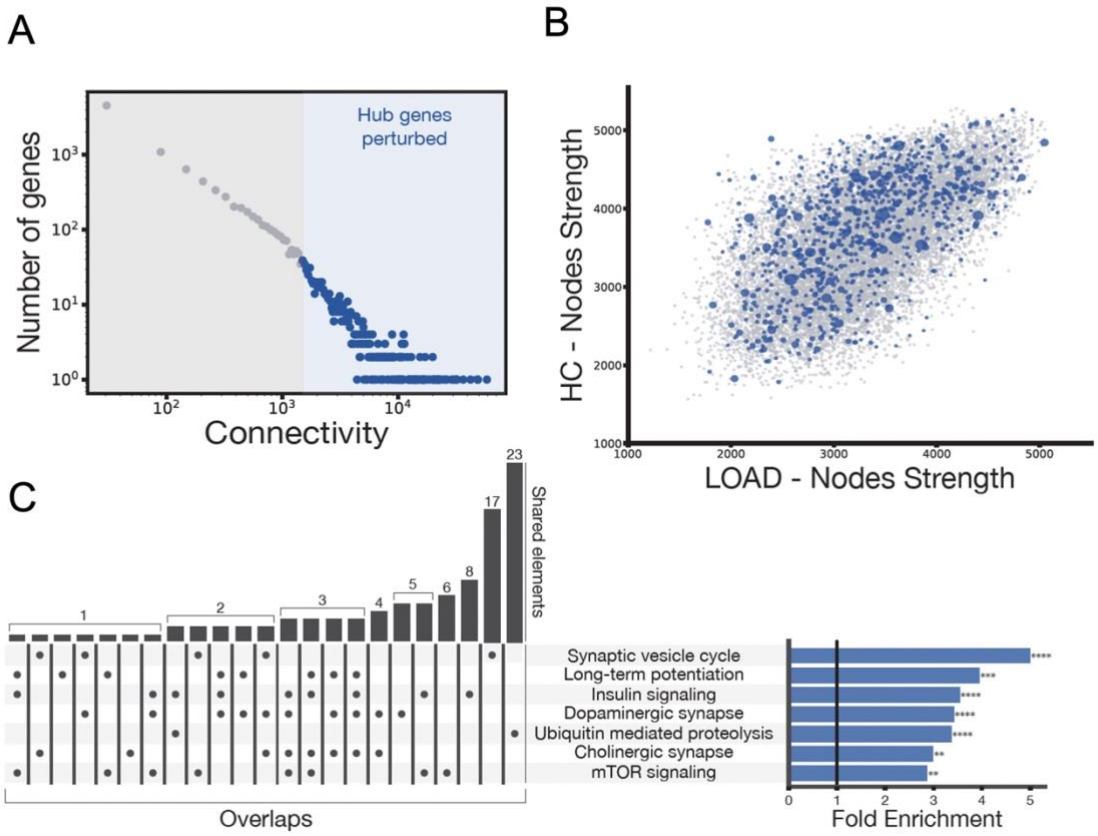

Figure S2. A network-based transcriptome-wide association study (nTWAS) identifies a set of genes and biological pathways with progressive transcriptomic dysregulation in Alzheimer's disease. (**A**) Distribution of the genes as a function of their connectivity with other genes in the perturbation network. The threshold identifies 10% of the genes in the perturbation network as hub genes. (**B**) Hub genes (blue dots, with size proportional to their connectivity) involved in the perturbed motifs. The scatter plot, representing the node centrality for all the genes in the transcriptome (measured by the node strength, see SI Methods) shows how the hub genes retrieved by nTWAS and majorly perturbed in disease were not the most intrinsically connected nodes of the network. (**C**) Enrichment analysis using the hub genes mapped onto KEGG pathways. Signalling and degradation pathways were found to be significantly enriched (right panel), with several genes found to be specific for the pathways of interest in the domino plot (left panel). Significance was calculated with Fisher's exact test, with the transcriptome as a background, and corrected with a Bonferroni multiple hypothesis testing correction **p < 0.01, ***p < 0.001, ****p < 0.0001.

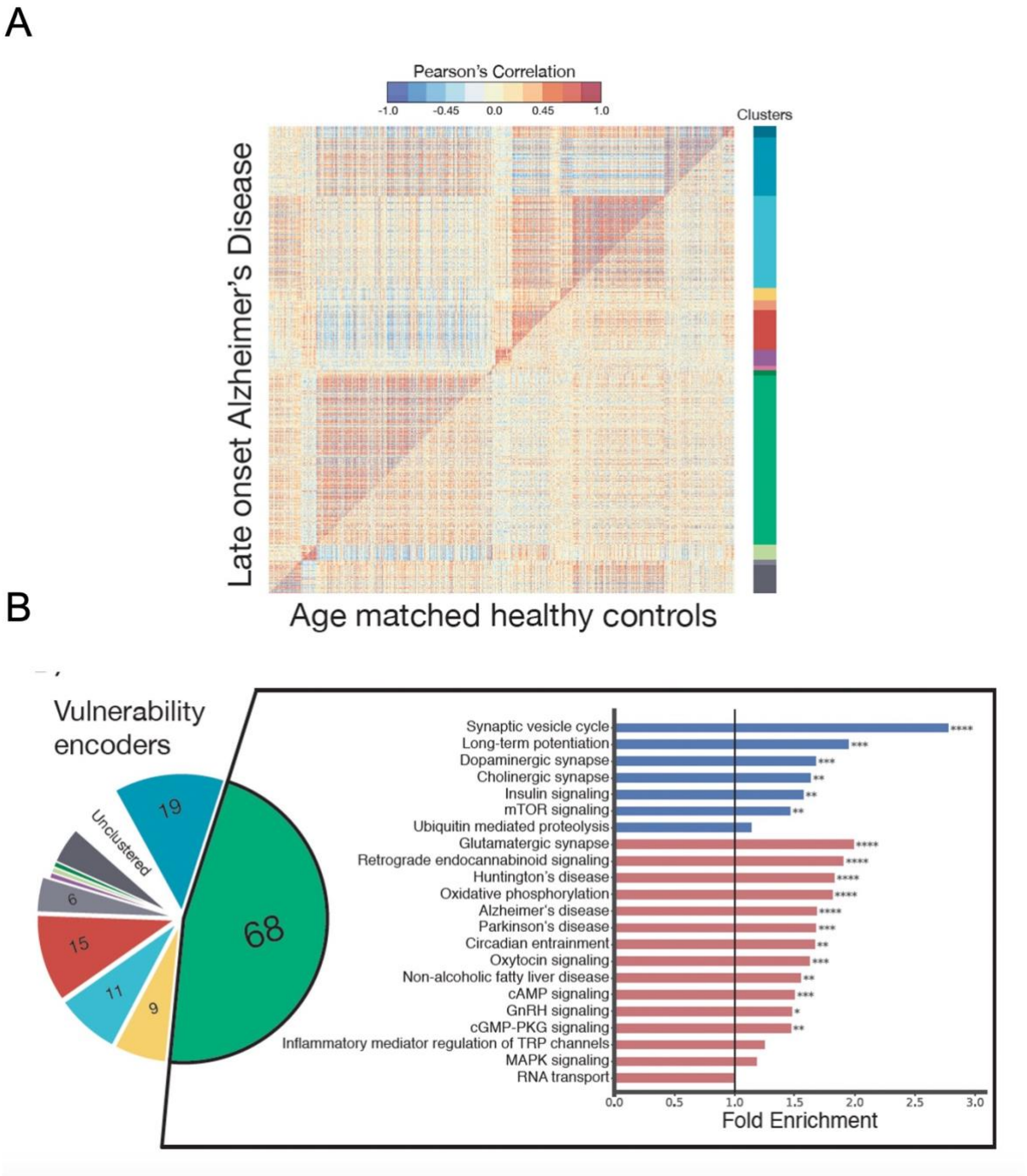

Figure S3. A differential co-expression clustering analysis reveals biological processes consistent with those identified using nTWAS. (**A**) Differential co-expression analysis conducted with DiffCoEx algorithm. Clusters of tightly differentially co-expressed genes between LOAD patients and healthy controls are reported and associated with colours identifying different modules. (**B**) Cluster membership of the vulnerability encoder genes (left panel) and KEGG pathways (with pathways corresponding to the GGS and nTWAS subsets reported in the red and blue region, respectively) mapped from the cluster showing highest membership. The statistical significance of the fold enrichment was computed using Fisher's exact test, with a Bonferroni multiple hypothesis testing correction *$p < 0.05$, **$p < 0.01$, ***$p < 0.001$, ****$p < 0.0001$.

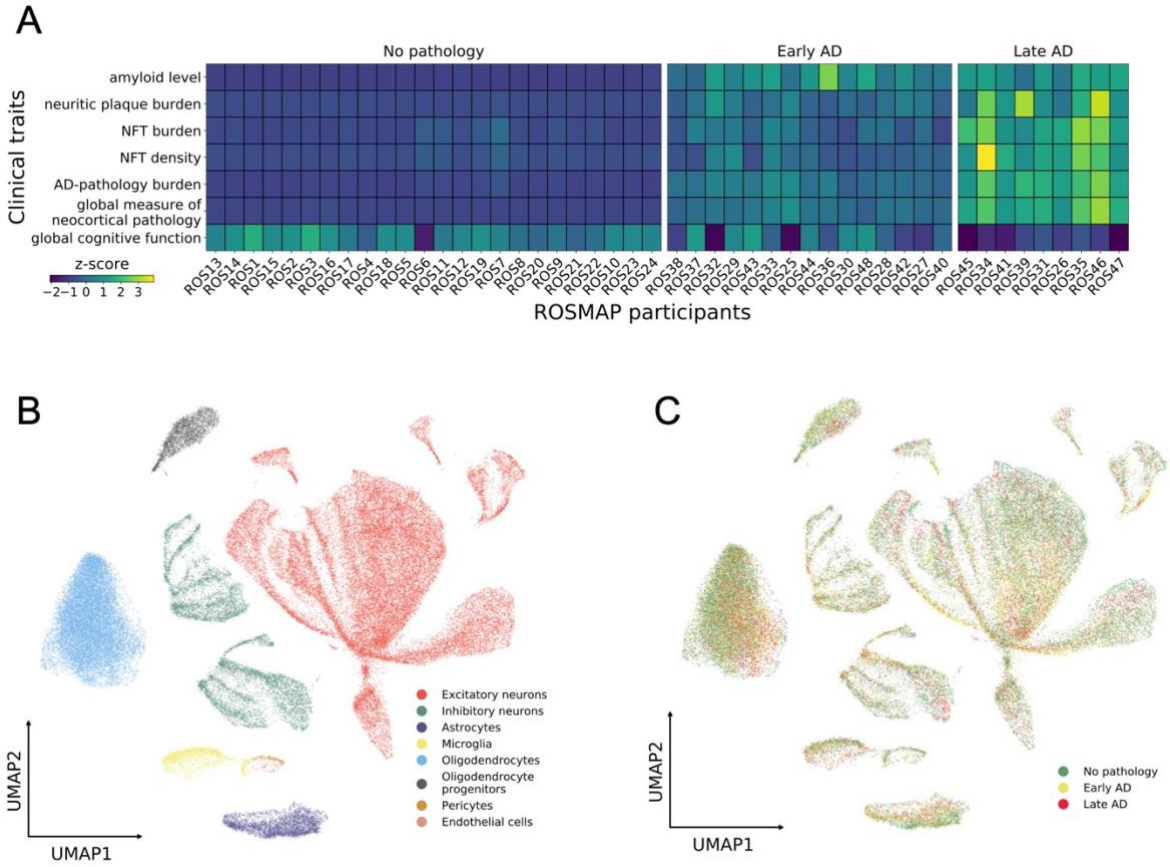

Figure S4. Cell-type annotation and donor stratification in ROSMAP single-nucleus RNA-seq data. (**A**) Grouping of the ROSMAP cohort according to AD clinical readouts. Phenotypic K-means clustering of the 48 individuals from the ROSMAP study (columns), identified by their IDs, using the clinico-pathological observations (rows), measuring the total amyloid level, the neuritic plaque burden, the neurofibrillary tangles burden, and their density, the overall pathological burden, the overall neocortical measure of the pathological state, and the global cognitive function. Z-scored values are shown. (**B,C**) UMAP visualisation of the cell nuclei, with the nuclei coloured according to their cell types (B) and disease stage (C). Eight clusters corresponding to major cell types were identified.

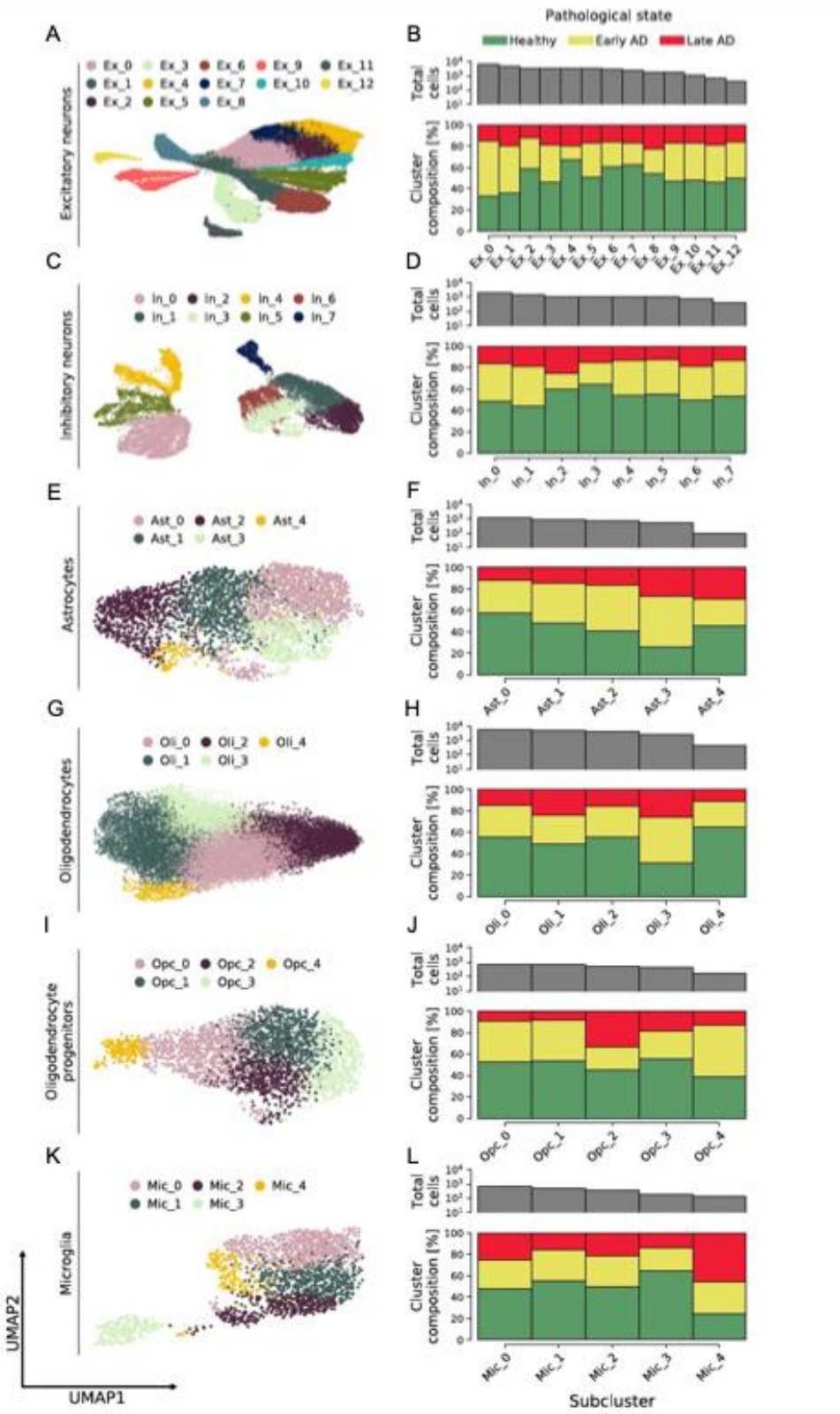

Figure S5. Louvain graph-clustering identifies multiple subclusters across major cell types. Results of the Louvain network-based clustering on the main cell types. **(A,C,E,G,I,K)** 2D UMAP embedding of the subpopulations. **(B,D,F,H,J,L)** Distribution of nuclei by donor group (control/early/late AD), with the total number of cell nuclei belonging to each cluster reported in the top panel.

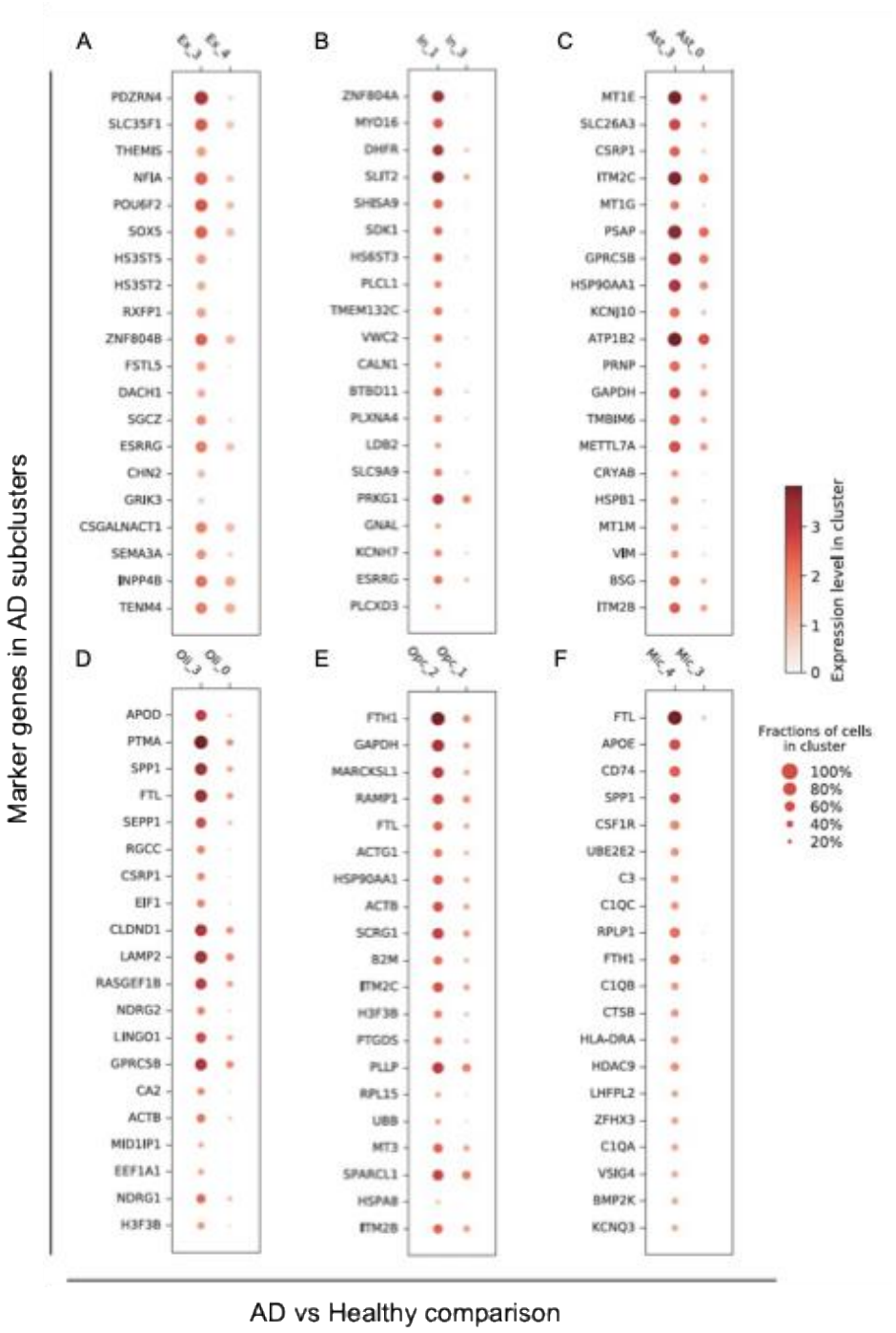

Figure S6. Subpopulations of cells enriched in pathological samples express genes associated with neurodegeneration and processes responsible for protein homeostasis. (A-F) The top 20 marker genes for 6 sub-clusters, one for each cell type, most significantly enriched for nuclei from AD donors (left column in each dotplot) compared to the subpopulation with highest enrichment in nuclei from healthy individuals (right column in each dotplot), within the same cell-type cluster, are showed. (A), excitatory neurons (Ex); (B), inhibitory neurons (In); (C), astrocytes (Ast); (D), oligodendrocytes (Oli); (E), oligodendrocyte progenitors (Opc); (F), microglia (Mic). The size of each dot indicates the fraction of cells expressing that gene inside the cluster, while the colour indicates the log-scaled average expression inside the cluster.

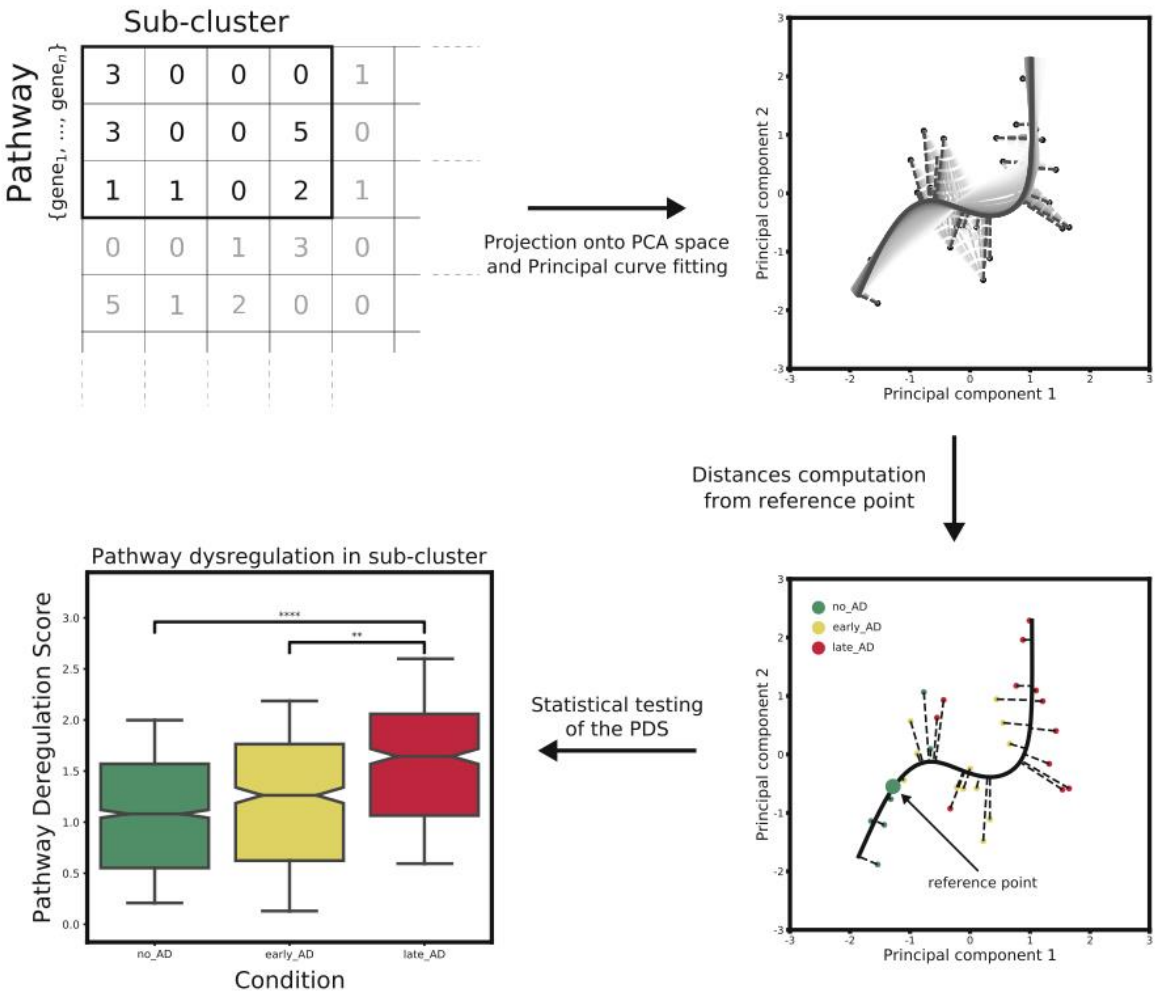

Figure S7. Pathifier analysis of AD pathways. To quantify pathway-level divergence in AD-labelled vs control-labelled nuclei, the gene expression matrix was iteratively transformed into subsets by selecting the matrix corresponding to a specific sub-cluster and a pathway (top left panel). The sub-matrix was then projected onto a lower dimensional space, i.e. the one generated with principal components analysis (PCA), and a principal curve was fitted to the data (the shading shows different iterations of the principal curve calculations to convergence, and the dashed lines the orthogonal projections of the samples onto the iterated curves) (top right panel). The Euclidean distances from a reference point (i.e. the average of the normal samples) of all the samples were then computed, with the indicating the donor group (control/early/late AD), called pathways deregulation scores (PDS) (bottom right panel). Ultimately, a statistical test was performed to test whether the pathway could separate samples associated with different pathological conditions along the principal curve (bottom left panel).

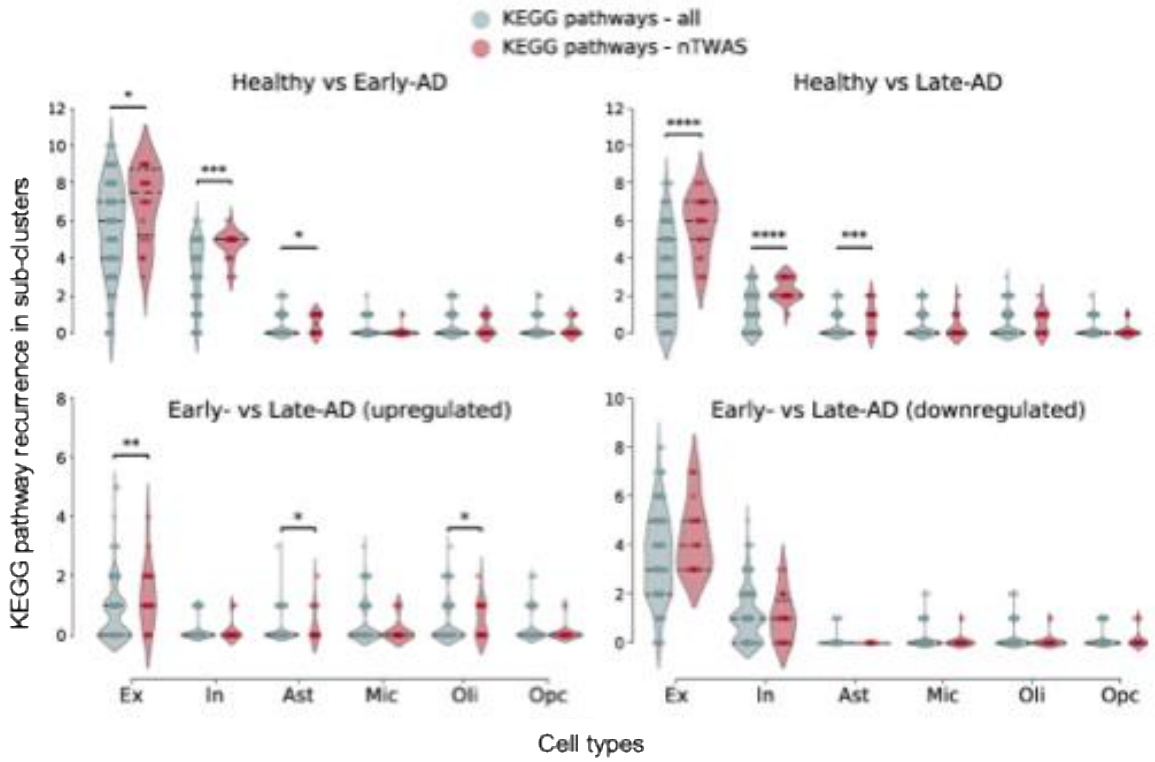

Figure S8. Comparison between the recurrence of the KEGG pathways and its nTWAS subset in all the cell subpopulations in AD stages. The number of times a pathway perturbation was found to be statistically significant within the subpopulations of each cell type (x axes) is reported. The distributions of all KEGG pathways (in grey) and of the nTWAS pathways (in red) are reported for each comparison in each main cell type. The median and interquartile range (IQR) are reported for each distribution with dashed lines. ****$p \leq 0.0001$, ***$p \leq 0.001$, **$p \leq 0.01$, *$p \leq 0.05$, one-sided Mann-Whitney U test with Bonferroni correction for multiple hypothesis testing.

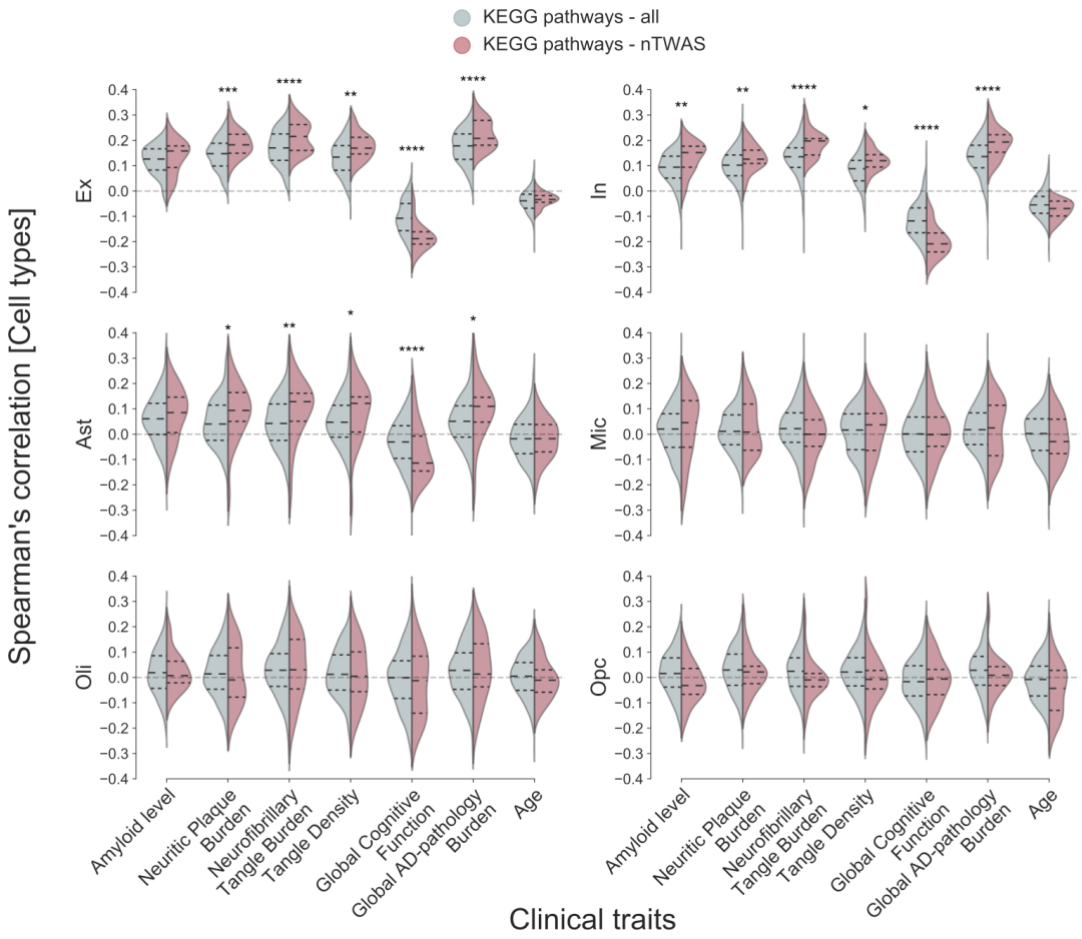

Figure S9. nTWAS pathway dysregulation scores correlate with clinico-pathological traits in neurons and astrocytes. Distributions of the median Spearman's correlation coefficients in the main cell types between the KEGG pathways (grey) and its nTWAS subset (red) and the clinico-pathological traits, reported on the x-axes. The median and interquartile range (IQR) are reported for each distribution with dashed lines. ****p ≤ 0.0001, ***p ≤ 0.001, **p ≤ 0.01, *p ≤ 0.05, one-sided Mann-Whitney U test with Bonferroni correction for multiple hypothesis testing.

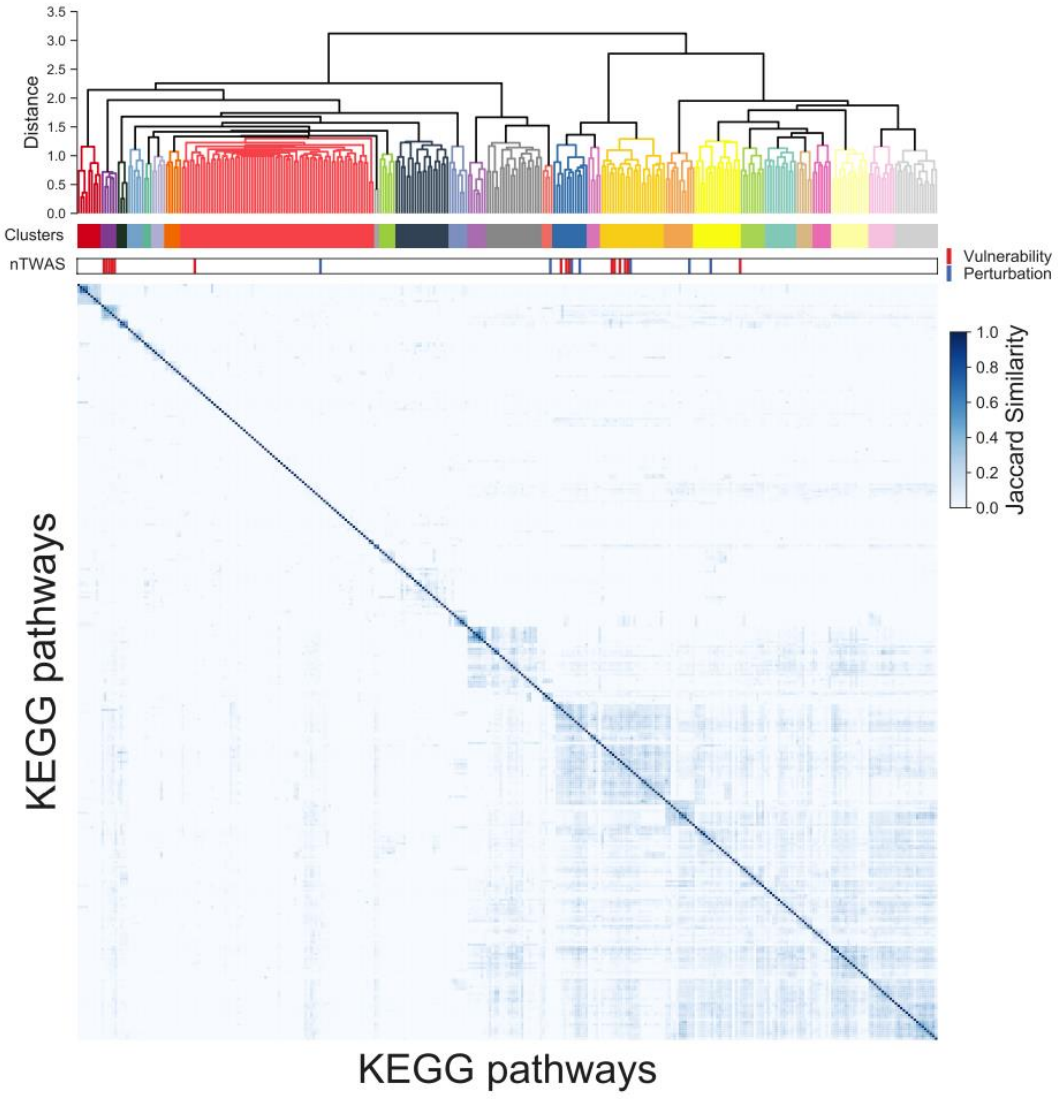

Figure S10. nTWAS pathways organise in specific clusters within KEGG annotations. Hierarchical clustering of the KEGG pathways based on the fraction of genes shared amongst them. The dendrogram shows the distances between the clusters. The similarity matrix shows the fraction of shared genes measured by the Jaccard similarity score. Position of the nTWAS pathways within the clusters is shown by the vertical bars, with those encoding for the vulnerability to AD identified by the red bars, and those associated with the perturbations occurring in disease reported in blue.

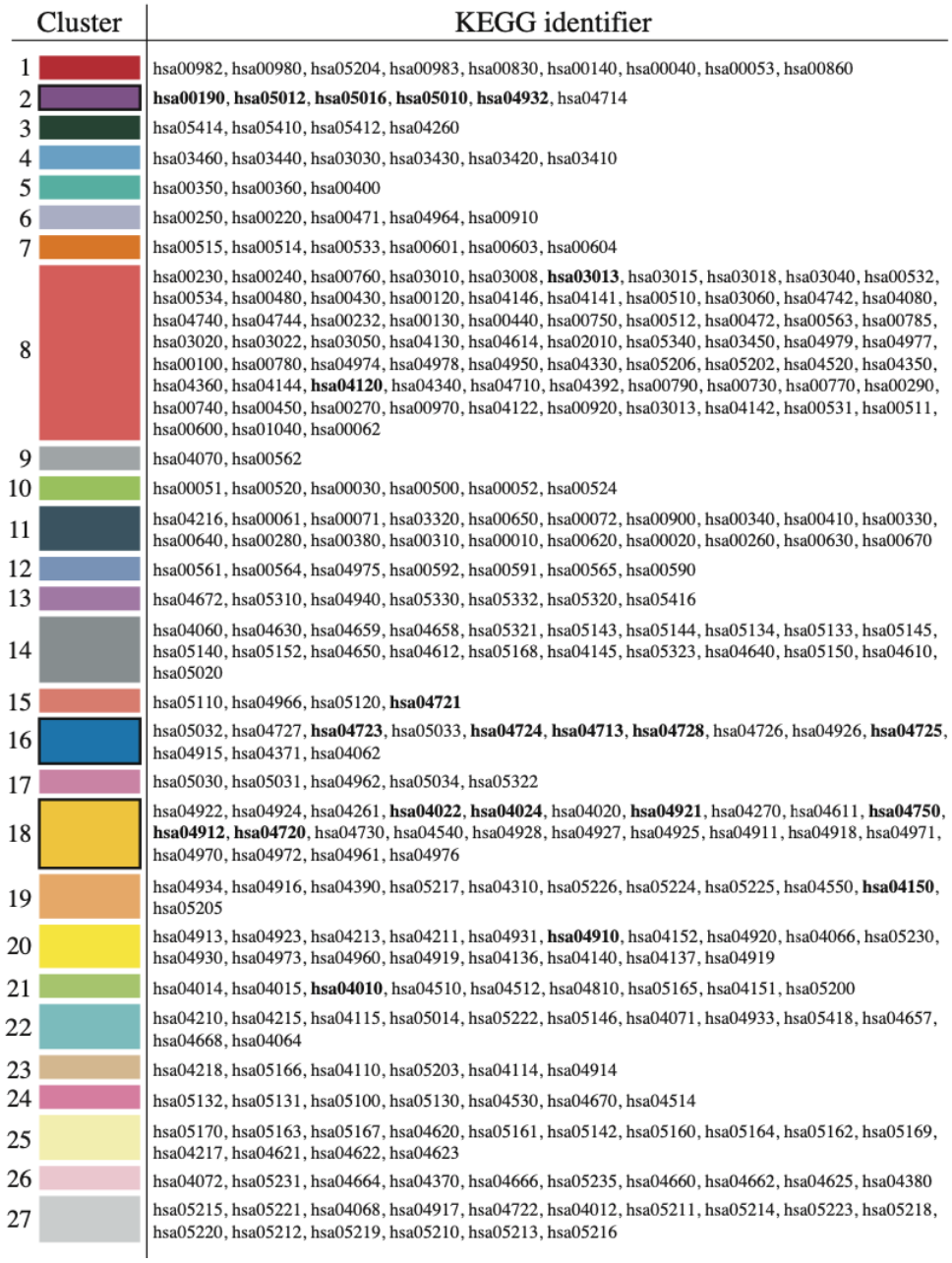

Cluster	KEGG identifier
1	hsa00982, hsa00980, hsa05204, hsa00983, hsa00830, hsa00140, hsa00040, hsa00053, hsa00860
2	**hsa00190**, **hsa05012**, **hsa05016**, **hsa05010**, **hsa04932**, hsa04714
3	hsa05414, hsa05410, hsa05412, hsa04260
4	hsa03460, hsa03440, hsa03030, hsa03430, hsa03420, hsa03410
5	hsa00350, hsa00360, hsa00400
6	hsa00250, hsa00220, hsa00471, hsa04964, hsa00910
7	hsa00515, hsa00514, hsa00533, hsa00601, hsa00603, hsa00604
8	hsa00230, hsa00240, hsa00760, hsa03010, hsa03008, **hsa03013**, hsa03015, hsa03018, hsa03040, hsa00532, hsa00534, hsa00480, hsa00430, hsa00120, hsa04146, hsa04141, hsa00510, hsa03060, hsa04742, hsa04080, hsa04740, hsa04744, hsa00232, hsa00130, hsa00440, hsa00750, hsa00512, hsa00472, hsa00563, hsa00785, hsa03020, hsa03022, hsa03050, hsa04130, hsa04614, hsa02010, hsa05340, hsa03450, hsa04979, hsa04977, hsa00100, hsa00780, hsa04974, hsa04978, hsa04950, hsa04330, hsa05206, hsa05202, hsa04520, hsa04350, hsa04360, hsa04144, **hsa04120**, hsa04340, hsa04710, hsa04392, hsa00790, hsa00730, hsa00770, hsa00290, hsa00740, hsa00450, hsa00270, hsa00970, hsa04122, hsa00920, hsa03013, hsa04142, hsa00531, hsa00511, hsa00600, hsa01040, hsa00062
9	hsa04070, hsa00562
10	hsa00051, hsa00520, hsa00030, hsa00500, hsa00052, hsa00524
11	hsa04216, hsa00061, hsa00071, hsa03320, hsa00650, hsa00072, hsa00900, hsa00340, hsa00410, hsa00330, hsa00640, hsa00280, hsa00380, hsa00310, hsa00010, hsa00620, hsa00020, hsa00260, hsa00630, hsa00670
12	hsa00561, hsa00564, hsa04975, hsa00592, hsa00591, hsa00565, hsa00590
13	hsa04672, hsa05310, hsa04940, hsa05330, hsa05332, hsa05320, hsa05416
14	hsa04060, hsa04630, hsa04659, hsa04658, hsa05321, hsa05143, hsa05144, hsa05134, hsa05133, hsa05145, hsa05140, hsa05152, hsa04650, hsa04612, hsa05168, hsa04145, hsa05323, hsa04640, hsa05150, hsa04610, hsa05020
15	hsa05110, hsa04966, hsa05120, **hsa04721**
16	hsa05032, hsa04727, **hsa04723**, hsa05033, **hsa04724**, **hsa04713**, **hsa04728**, hsa04726, hsa04926, **hsa04725**, hsa04915, hsa04371, hsa04062
17	hsa05030, hsa05031, hsa04962, hsa05034, hsa05322
18	hsa04922, hsa04924, hsa04261, **hsa04022**, **hsa04024**, hsa04020, **hsa04921**, hsa04270, hsa04611, **hsa04750**, **hsa04912**, **hsa04720**, hsa04730, hsa04540, hsa04928, hsa04927, hsa04925, hsa04911, hsa04918, hsa04971, hsa04970, hsa04972, hsa04961, hsa04976
19	hsa04934, hsa04916, hsa04390, hsa05217, hsa04310, hsa05226, hsa05224, hsa05225, hsa04550, **hsa04150**, hsa05205
20	hsa04913, hsa04923, hsa04213, hsa04211, hsa04931, **hsa04910**, hsa04152, hsa04920, hsa04066, hsa05230, hsa04930, hsa04973, hsa04960, hsa04919, hsa04136, hsa04140, hsa04137, hsa04919
21	hsa04014, hsa04015, **hsa04010**, hsa04510, hsa04512, hsa04810, hsa05165, hsa04151, hsa05200
22	hsa04210, hsa04215, hsa04115, hsa05014, hsa05222, hsa05146, hsa04071, hsa04933, hsa05418, hsa04657, hsa04668, hsa04064
23	hsa04218, hsa05166, hsa04110, hsa05203, hsa04114, hsa04914
24	hsa05132, hsa05131, hsa05100, hsa05130, hsa04530, hsa04670, hsa04514
25	hsa05170, hsa05163, hsa05167, hsa04620, hsa05161, hsa05142, hsa05160, hsa05164, hsa05162, hsa05169, hsa04217, hsa04621, hsa04622, hsa04623
26	hsa04072, hsa05231, hsa04664, hsa04370, hsa04666, hsa05235, hsa04660, hsa04662, hsa04625, hsa04380
27	hsa05215, hsa05221, hsa04068, hsa04917, hsa04722, hsa04012, hsa05211, hsa05214, hsa05223, hsa05218, hsa05220, hsa05212, hsa05219, hsa05210, hsa05213, hsa05216

Figure S11. List of clusters of KEGG pathways. The clusters (colour-coded) and the KEGG identifiers corresponding to the pathways contained in each cluster. nTWAS pathways are in bold; hsa00190: Oxidative phosphorylation; hsa05012: Parkinson's Disease (PD); hsa05016: Huntington's Disease (HD); hsa05010: Alzheimer's disease (AD); hsa04932: Non-alcoholic fatty liver disease (NAFLD); hsa03013: RNA transport; hsa04120: Ubiquitin mediated proteolysis; hsa04721: Synaptic vesicle cycle; hsa04723: Retrograde endocannabinoid signaling; hsa04724: Glutamatergic synapse; hsa04713: Circadian en- trainment; hsa04728: Dopaminergic synapse; hsa04725: Cholinergic synapse; hsa04022: cGMP-PKG signaling pathway; hsa04024: cAMP signaling pathway; hsa04921: Oxytocin signaling pathway; hsa04750: Inflammatory mediator regulation of TRP channels; hsa04912: GnRH signaling pathways; hsa04720: Long-term potentiaion; hsa04150: mTOR signaling pathway; hsa04910: Insulin signaling pathway; hsa04010: MAPK signaling pathway. The clusters highlighted in black are enriched in nTWAS pathways.

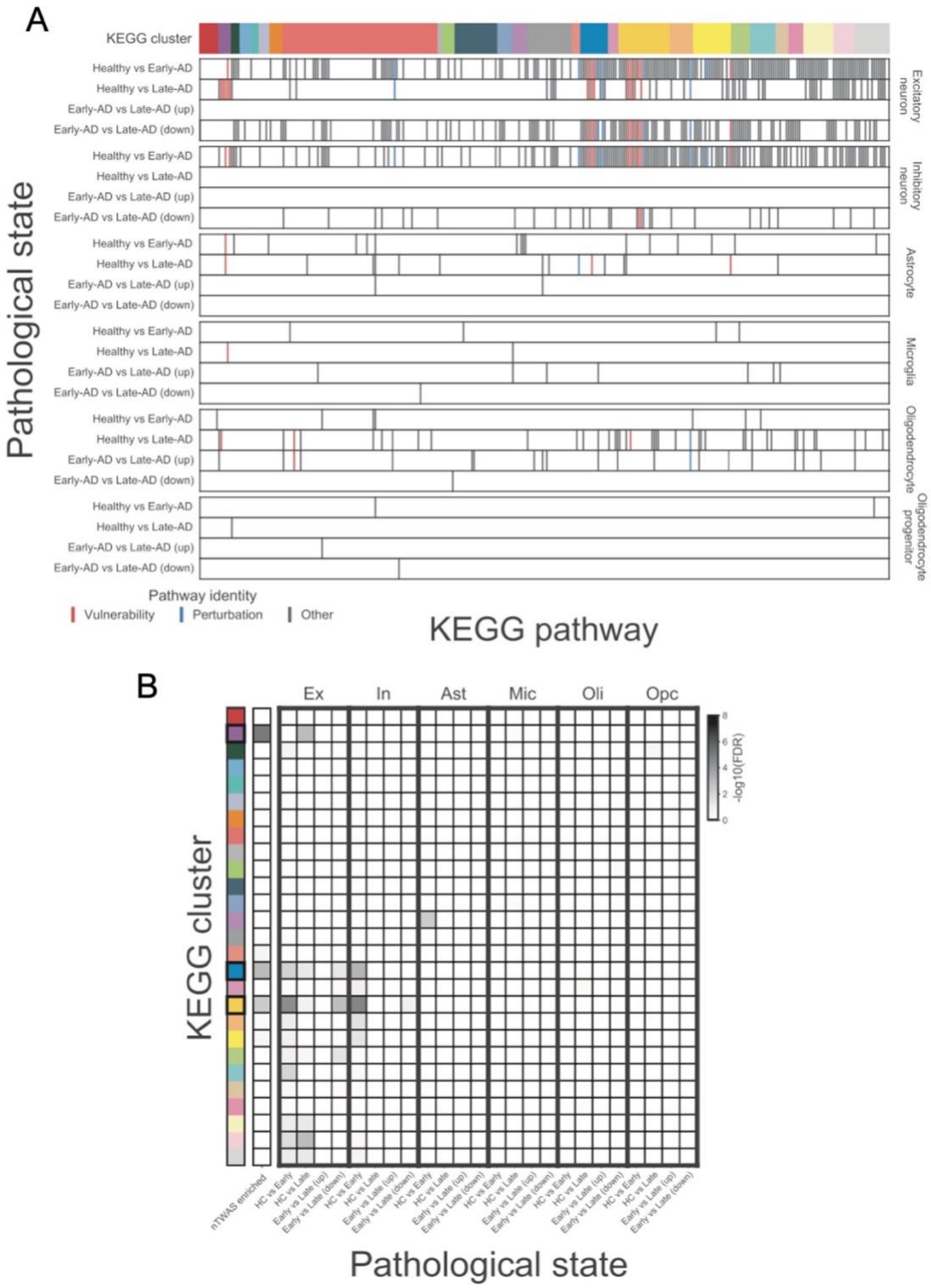

Figure S12. Clusters of KEGG pathways containing the nTWAS pathways are preferentially perturbed in neuronal cells. (A) Dysregulated pathways belonging to each KEGG cluster, are reported for each cell type, and for each comparison within the cell types. Each vertical bar represents a pathway; nTWAS pathways are highlighted in red or blue according to their nTWAS classification, while non-nTWAS pathways are shown in black. **(B)** Statistical enrichment of the different KEGG clusters in the different conditions, within each cell type. The first column corresponds to the enrichment of each cluster in nTWAS pathways. Enrichment was computed using Fisher's exact test, with Bonferroni correction for multiple hypothesis testing.

Figure S13. Cell type-specific perturbation of nTWAS-enriched KEGG pathways across AD stages. Heatmaps show the significance of pathway deregulation (-log10 FDR) across cell-type subclusters in pairwise disease-stage comparisons: Healthy vs. Early-AD, Healthy vs. Late-AD, Early-AD vs. Late-AD (upregulated), and Early-AD vs. Late-AD (downregulated). Pathways correspond to those previously identified by nTWAS as associated with AD risk in the nTWAS analysis. Each column represents a subcluster within a major brain cell type (Astrocytes, Excitatory neurons, Inhibitory neurons, Microglia, Oligodendrocytes, OPCs, Pericytes, Endothelial cells). Blue shading intensity reflects statistical significance of pathway perturbation, with darker shades indicating stronger associations. Prominent early changes in excitatory neuron subclusters include dysregulation of the synaptic vesicle cycle and ubiquitin-mediated proteolysis pathways, which remain altered when comparing early to late AD. In contrast, glial perturbations are more stage-dependent, becoming more prominent in late disease.

Cell type	Sub-cluster	Number of cells
Ex	Ex_0	6343
	Ex_1	4392
	Ex_2	3452
	Ex_3	3162
	Ex_4	3147
	Ex_5	3135
	Ex_6	2941
	Ex_7	2601
	Ex_8	1823
	Ex_9	1675
	Ex_10	1130
	Ex_11	710
	Ex_12	444
In	In_0	2183
	In_1	1586
	In_2	1152
	In_3	1052
	In_4	1028
	In_5	1015
	In_6	764
	In_7	412
Ast	Ast_0	1157
	Ast_1	863
	Ast_2	717
	Ast_3	558
	Ast_4	96
Mic	Mic_0	684
	Mic_1	518
	Mic_2	378
	Mic_3	196
	Mic_4	143
Oli	Oli_0	5961
	Oli_1	4906
	Oli_2	4209
	Oli_3	2740
	Oli_4	419
Opc	Opc_0	740
	Opc_1	718
	Opc_2	545
	Opc_3	457
	Opc_4	167

Figure S14. Cell-type and subcluster composition of the ROSMAP single-nucleus RNA-seq dataset. Summary of nuclei counts per major cell type and Louvain-derived transcriptional subcluster in the ROSMAP prefrontal cortex dataset (70,634 nuclei total after QC). Six broad cell classes (excitatory neurons (Ex), inhibitory neurons (In), astrocytes (Ast), microglia (Mic), oligodendrocytes (Oli), and OPCs) were further partitioned into refined subclusters. The table reports the number of nuclei assigned to each subcluster and was used as the basis for all downstream analyses of AD-associated pathway perturbations.

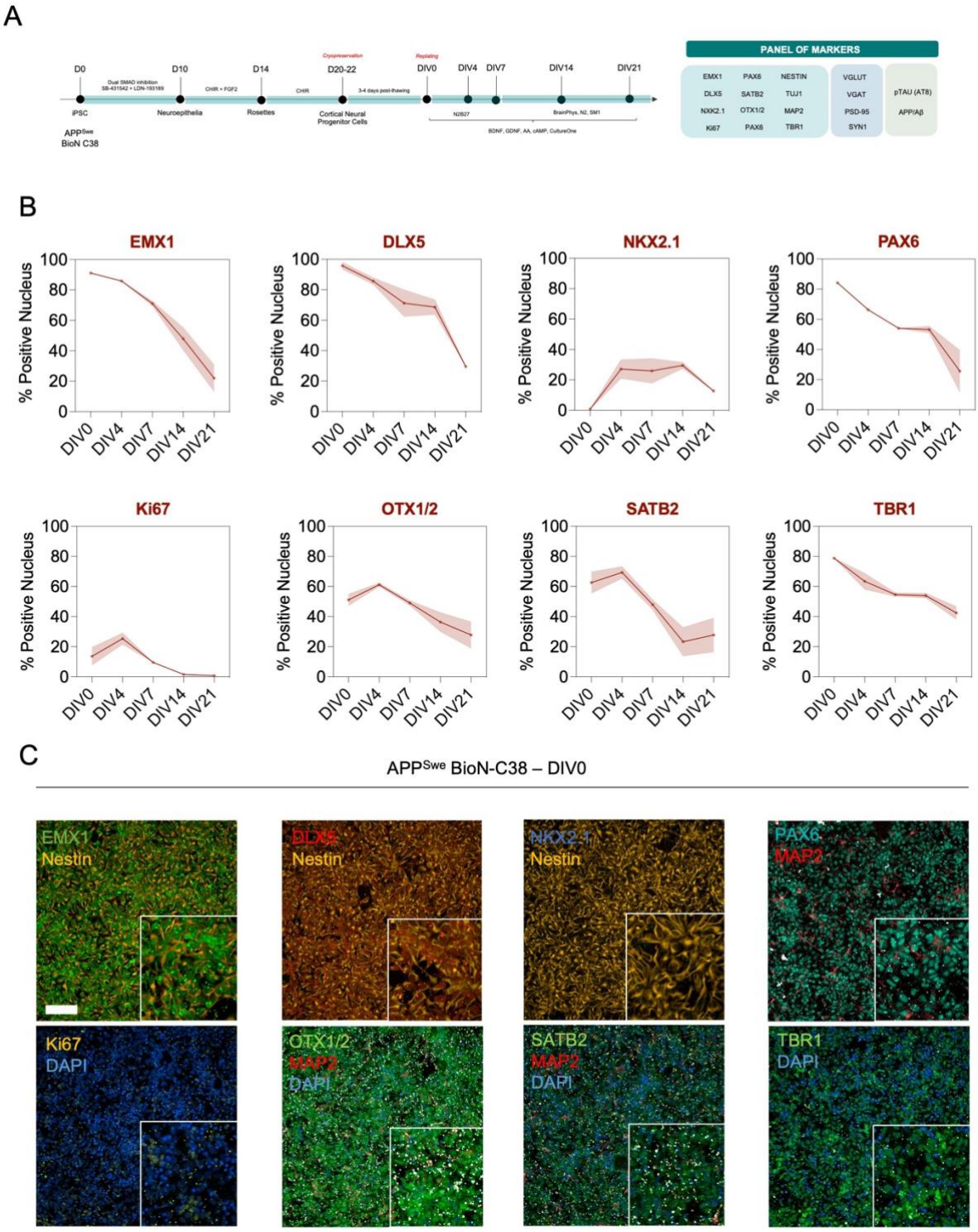

Figure S15. Quality control of APP^{Swe} cortical neural progenitor cells (NPCs) by immunocytochemistry. (A) Illustration of the differentiation protocol used in this work, which was adapted from a previously reported one [1]. hiPSCs are converted into neuroepithelia, followed by neural tube-like rosette formation and subsequent isolation of cortical NPCs, which then are differentiated to cortical glutamatergic neurons. The NPCs generation process takes 20-22 d. Following generation, high-purity cortical NPCs are cryopreserved in large batches to maintain population homogeneity and reduce experimental variability. **(B)** The phenotypic nature of cortical APP^{Swe} NPCs is characterised by assessing their enrichment in EMX1, DLX5, PAX6, OTX1/2 and SATB2

expression, which is expected to decrease upon differentiation to mature neurons. Absence of NKX2.1 (a marker of ventral forebrain interneuron progenitors [2]) was also indicative of the cortical identity of our NPCs. Ki67 was used as a marker to determine the percentage of mitotic cells in culture. Data are represented as the mean and standard error of the percentage of DAPI-positive nuclei that stained positive for the expression of each transcription factor. Expression was assessed by immunocytochemistry at DIV0 (NPC stage), DIV4, 7, 14 and 21 (n = 3). **(C)** Representative images showcasing the expression levels of each transcription factor at DIV0. Cells were also stained for DAPI (nuclei), nestin (cytoskeleton of progenitor cells) and MAP2 (dendritic marker of neuronal maturity). Scale bar = 100 μm.

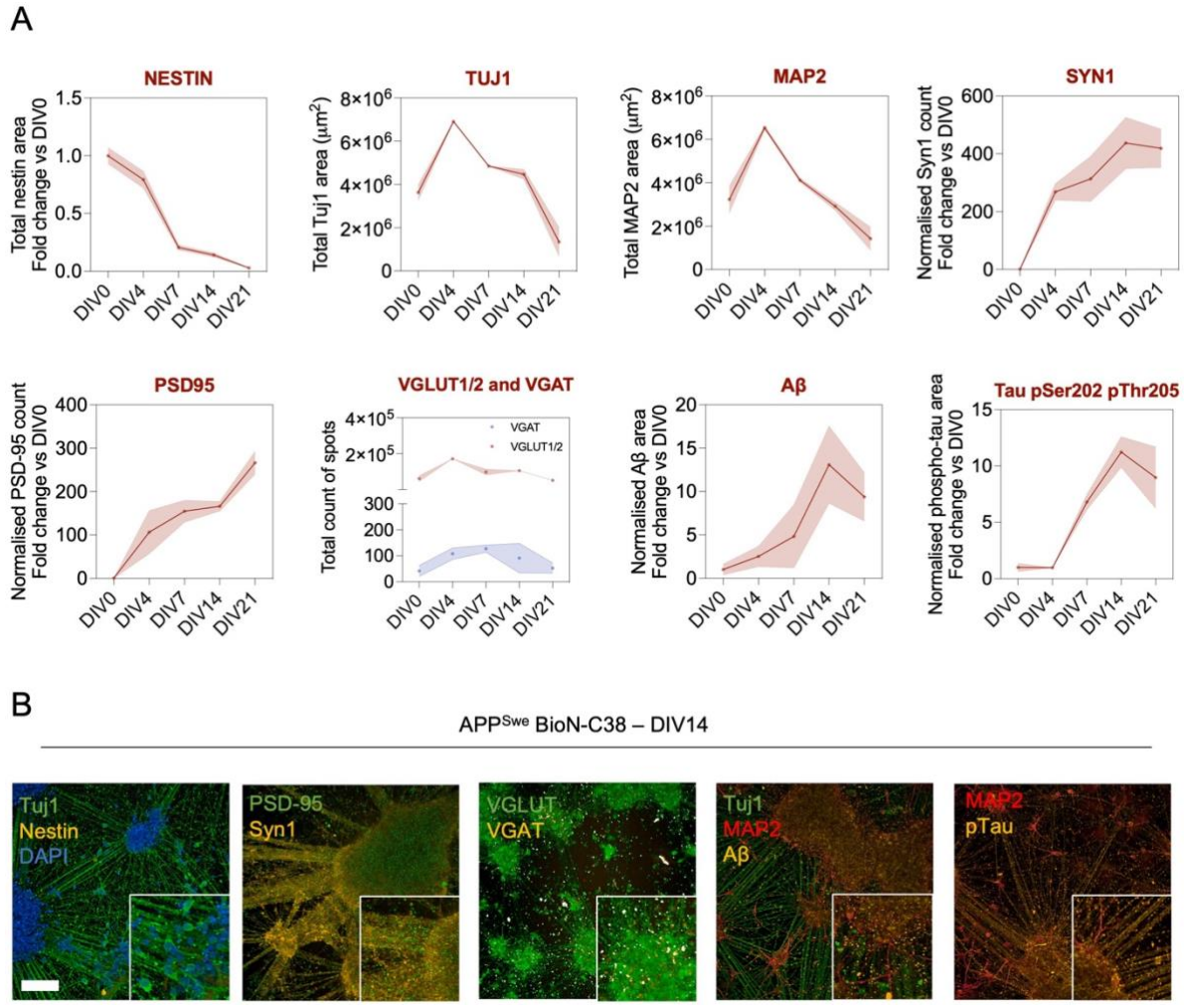

Figure S16. Quality control of APP^{Swe} cortical glutamatergic neurons by immunocytochemistry. **(A)** The phenotypic nature of cortical glutamatergic neurons derived from the BIONi010-C-38 iPSC clone is characterised by assessing: (i) the decrease in expression levels of the progenitor-specific marker nestin upon neuronal maturation, (ii) the expression of axonal (Tuj1) and dendritic (MAP2) markers, (iii) the increase in expression levels of pre-synaptic (Syn1) and post-synaptic (PSD-95) markers upon neuronal maturation, and (iv) the presence in expression of VGLUT1/2 (glutamatergic neurons) and absence in expression of VGAT (GABAergic neurons). We also assessed baseline Aβ- and phospho-tau-related signals in these cultures. Nestin, Tuj1 and MAP2 data are represented as the sum of the neuronal area stained positive for each marker. The expression levels of Syn1, PSD-95, VGLUT1/2, VGAT, Aβ and phospho-tau are reported as the total area or total spot count measured within axonal projections or dendrites, normalised respectively by the total Tuj1 or MAP2 area. **(B)** Representative images showing the expression levels of each marker at DIV14. Scale bar = 100 µm.

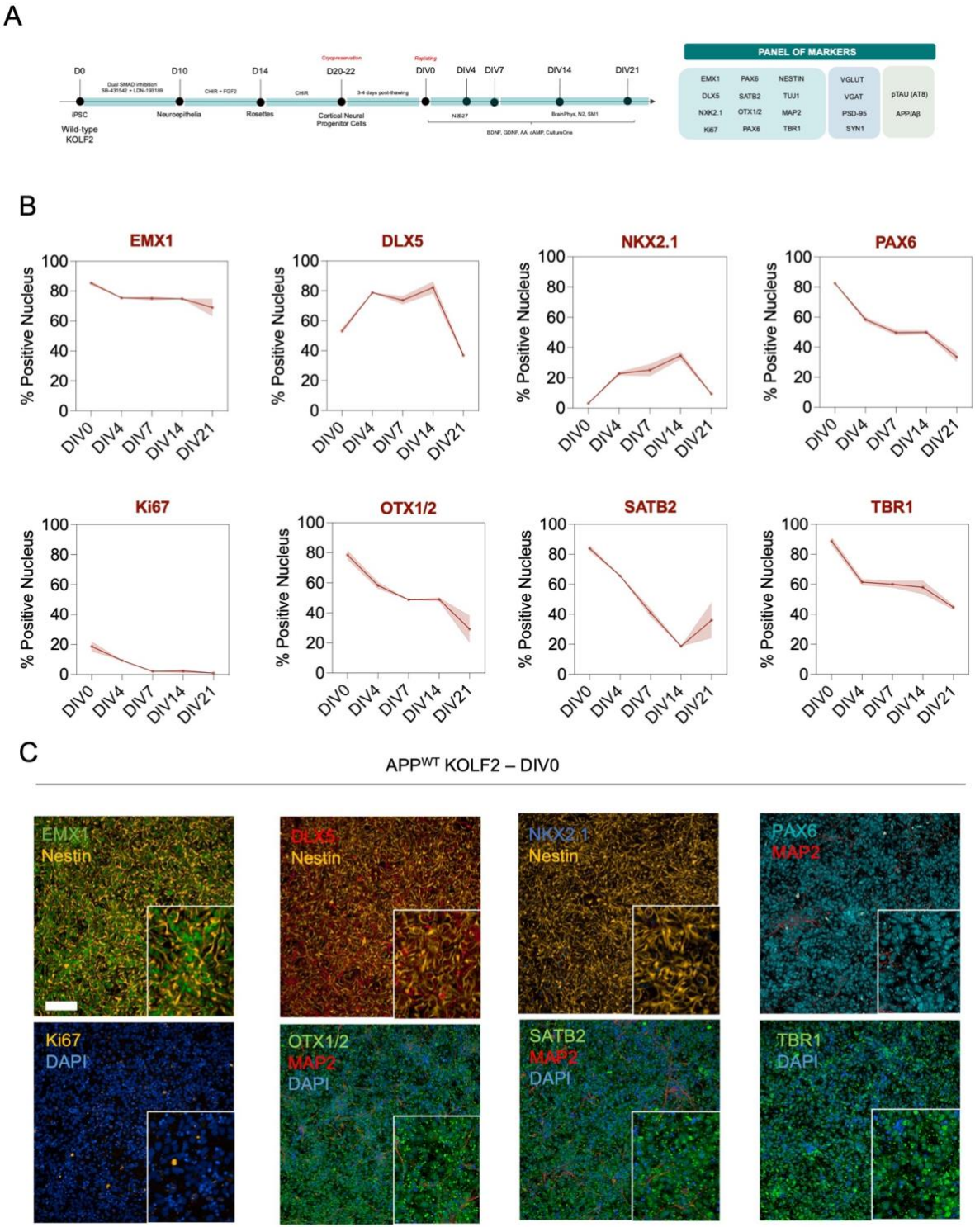

Figure S17. Quality control of APP^{WT} cortical neural progenitor cells (NPCs) by immunocytochemistry. (A) Illustration of the differentiation protocol used in this work, which was adapted from a previously reported one [1]. hiPSCs are converted into neuroepithelia, followed by neural tube-like rosette formation and subsequent isolation of cortical NPCs which are then differentiated to cortical glutamatergic neurons. NPCs generation process takes 20-22 days. Following generation, high-purity cortical NPCs are cryopreserved in large batches to maintain population homogeneity and reduce experimental variability. **(B)** The phenotypic nature of cortical APP^{WT} NPCs is characterised by assessing their enrichment in EMX1, DLX5, PAX6, OTX1/2 and SATB2

expression, which is expected to decrease upon differentiation to mature neurons. Absence of NKX2.1 levels (a marker of ventral forebrain interneuron progenitors [2]) was also indicative of the cortical identity of our NPCs. Ki67 was used as a marker to determine the percentage of mitotic cells in culture. Data are represented as the mean and standard error of the percentage of DAPI-positive nuclei that stained positive for the expression of each transcription factor. Expression was assessed by immunocytochemistry at DIV0 (NPC stage), DIV4, 7, 14 and 21 (n = 3). **(C)** Representative images showcasing the expression levels of each transcription factor at DIV0. Cells were also stained for DAPI (nuclei), nestin (cytoskeleton of progenitor cells) and MAP2 (dendritic marker of neuronal maturity). Scale bar = 100 μm.

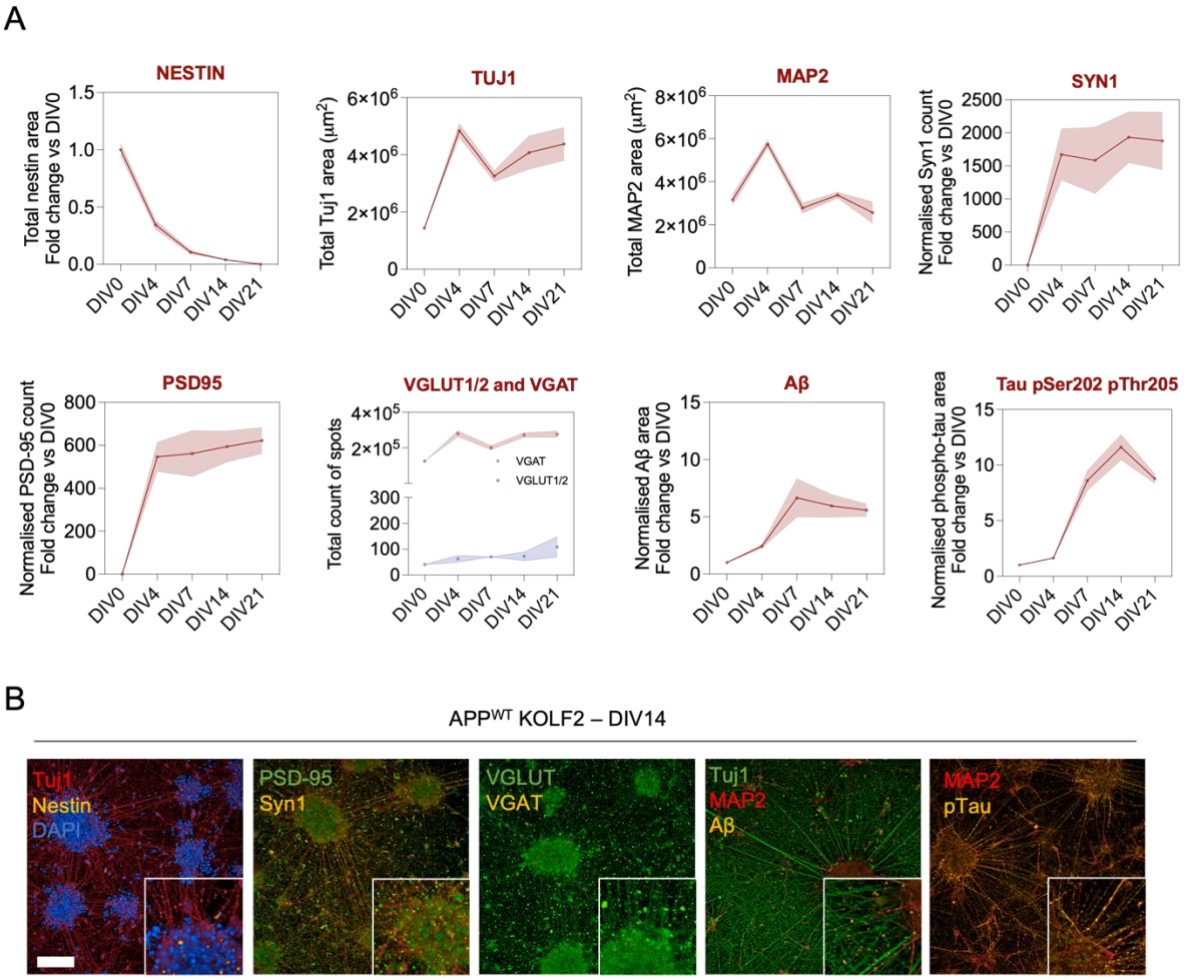

Figure S18. Quality control of APP^{WT} cortical glutamatergic neurons by immunocytochemistry. **(A)** The phenotypic nature of cortical glutamatergic neurons derived from the KOLF2.1 iPSC clone is characterised by assessing: (i) the decrease in expression levels of the progenitor-specific marker nestin upon neuronal maturation, (ii) the expression of axonal (Tuj1) and dendritic (MAP2) markers, (iii) the increase in expression levels of pre-synaptic (Syn1) and post-synaptic (PSD-95) markers upon neuronal maturation, and (iv) the presence in expression of VGLUT1/2 (glutamatergic neurons) and absence in expression of VGAT (GABAergic neurons). We also quantified baseline Aβ and phospho-tau signals in these cultures. Nestin, Tuj1 and MAP2 data are represented as the sum of the neuronal area stained positive for each marker. The expression levelsof Syn1, PSD-95, VGLUT1/2, VGAT, Aβ and phospho-tau are reported as the total area or total spot count measured within axonal projections or dendrites, normalised respectively by the total Tuj1 or MAP2 area. **(B)** Representative pictures showcasing the expression levels of each marker at DIV14. Scale bar = 100 µm.

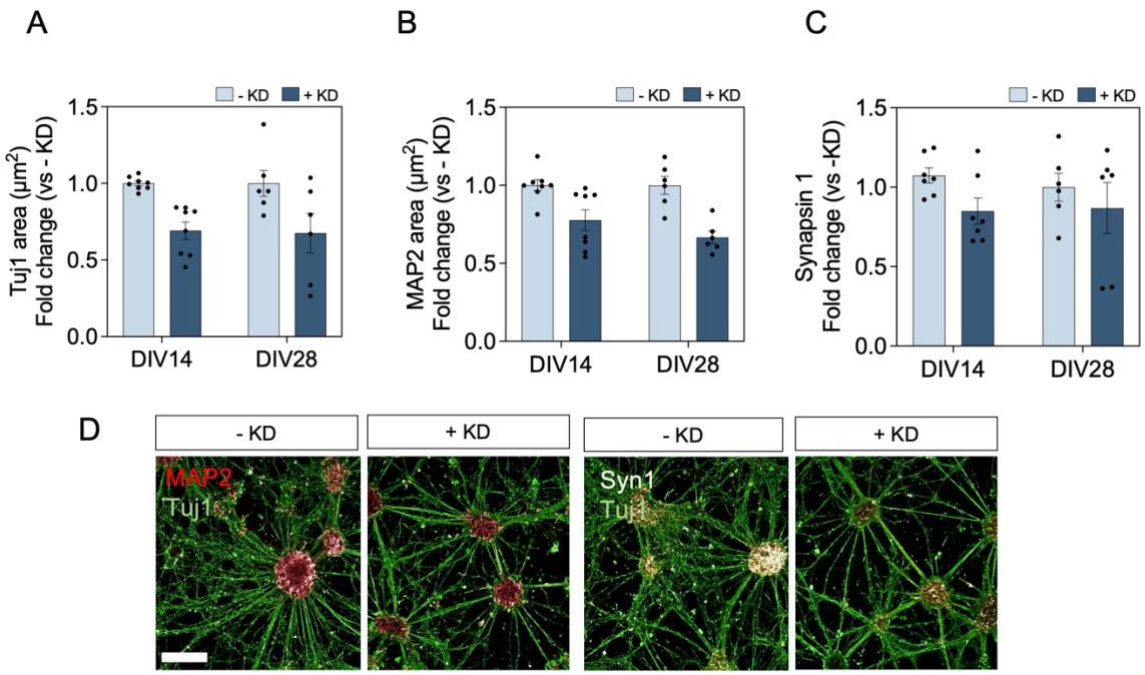

Figure S19. *FBXO2* downregulation is associated with mild reductions in neuronal structural and synaptic marker abundance in APP^{Swe} cortical neurons. (A-C) Quantification of neuronal structural and synaptic markers in APP^{Swe} cortical neurons subjected to early *FBXO2* knockdown (+KD) or scrambled control (-KD) at DIV14 and DIV28 (N = 2). **(A)** Tuj1^{+} axonal area, **(B)** MAP2^{+} dendritic area, and **(C)** Synapsin-1 (Syn1)$^{+}$ area are shown as fold change relative to -KD neurons. Early *FBXO2* downregulation results in slight reductions in axonal and dendritic markers and subtle decreases in synaptic area. **(D)** Representative immunofluorescence images showing MAP2 (red), Tuj1 (green), and Syn1 (yellow) in -KD and +KD neurons. Scale bar, 50 µm.

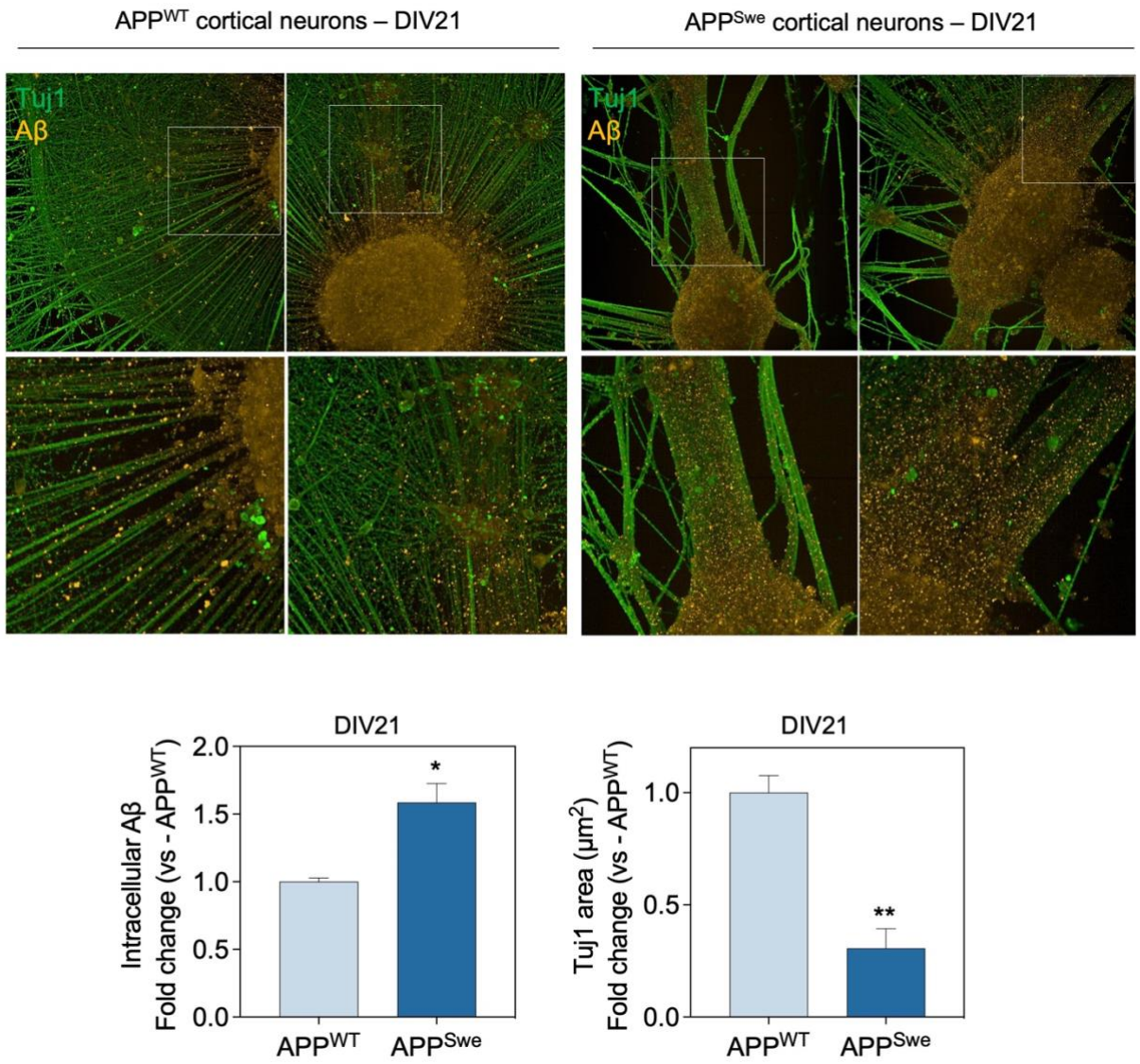

Figure S20. Differences in axonal distribution and Aβ content between APP^{WT} and APP^{Swe} cortical neurons. Representative images of APP^{WT} and APP^{Swe} cortical neurons differentiated for 21 days (DIV21), stained for axonal projections (Tuj1) and Aβ (W02). The images show that APP^{Swe} cortical neurons derived from the clone BIONi010-C-38, tend to form more clusters and thicker axonal projections as compared to the APP^{WT} cortical neurons derived from the KOLF2.1 clone. Therefore, clustering differences may cause APP^{Swe} neurons to exhibit a smaller total Tuj1 area not related to degeneration. Levels of total Aβ clusters, measured as the high intensity spots located along the Tuj1-positive area, were 1.5 times higher in APP^{Swe} neurons as compared to APP^{WT}. Statistical significance is indicated as: * $p<0.05$, ** $p<0.01$, determined by a t-test.

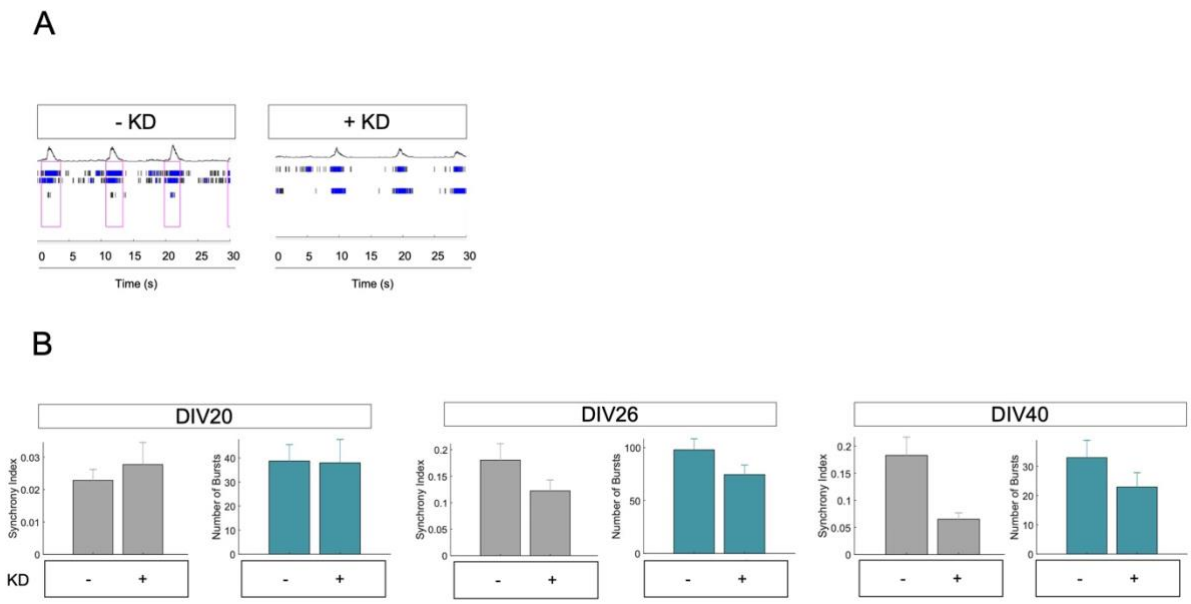

Figure S21. Electrophysiological activity of APP^{WT} neurons following early *FBXO2* downregulation. (A) Representative raster plots of spontaneous network activity recorded from multielectrode array (MEA) wells at DIV26 in APP^{WT} neurons transfected with scrambled control (-KD) or FBXO2 siRNAs (+KD). Each row corresponds to one electrode. Black ticks indicate individual spikes, blue ticks indicate bursts detected at a single electrode, and pink boxes mark synchronised bursts occurring across multiple electrodes. Neurons with downregulated *FBXO2* show a reduction in burst synchrony, consistent with impaired network coordination **(B)** Quantification of network synchrony and burst production at DIV20, DIV26 and DIV40. For each time point, the synchrony index (left plot) and number of bursts per recording (right plot) are shown for -KD and +KD neurons. Across maturation, *FBXO2* knockdown corresponded to mild and progressive impairments in burst synchrony and burst frequency, most evident at later stages. Data were obtained from 32 independent MEA wells per group.

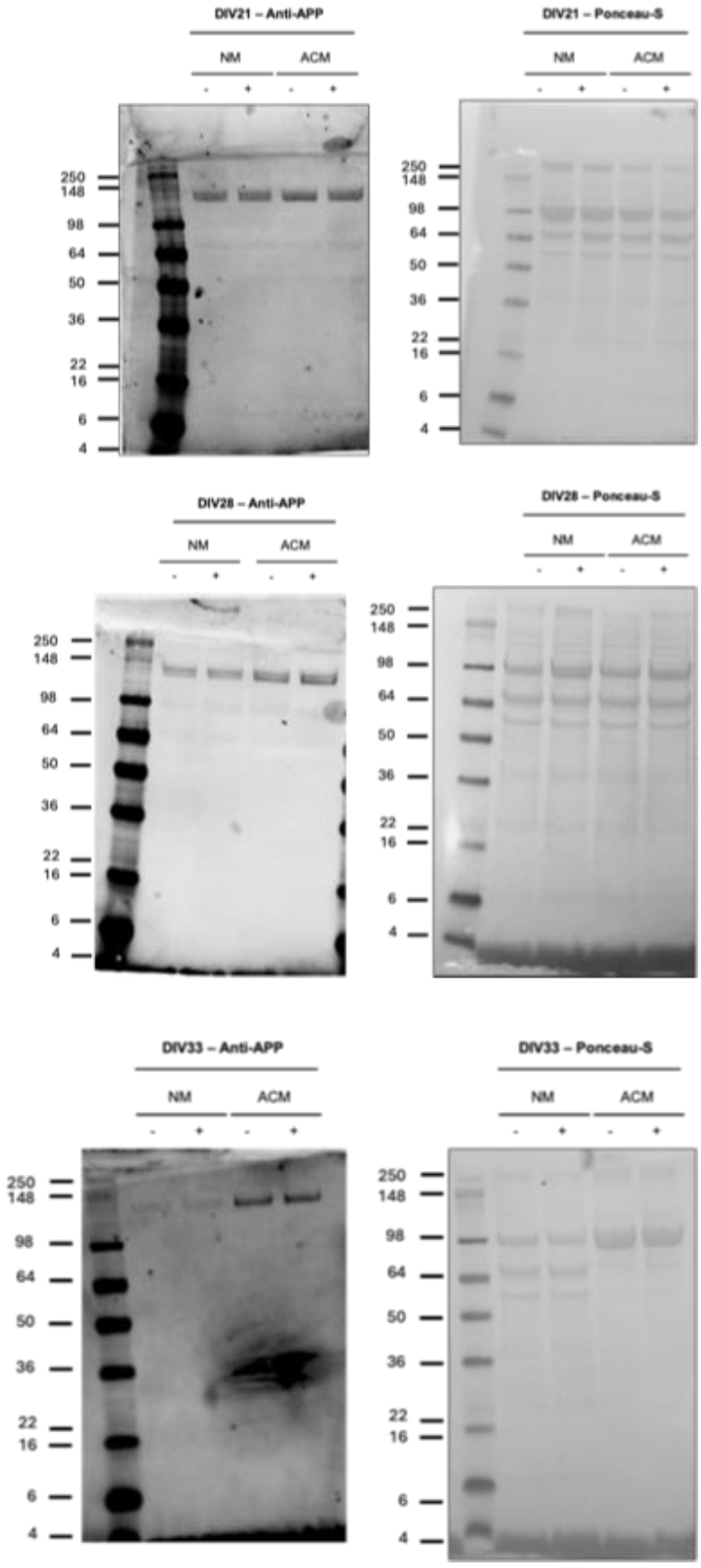

Figure S22. Western blots for APP and Ponceau-S stainings of NM and ACM treated neurons, pre-treated with ScrRNA (-) or FBXO2 (+) siRNAs. The antibody W02 was used to measure APP levels.

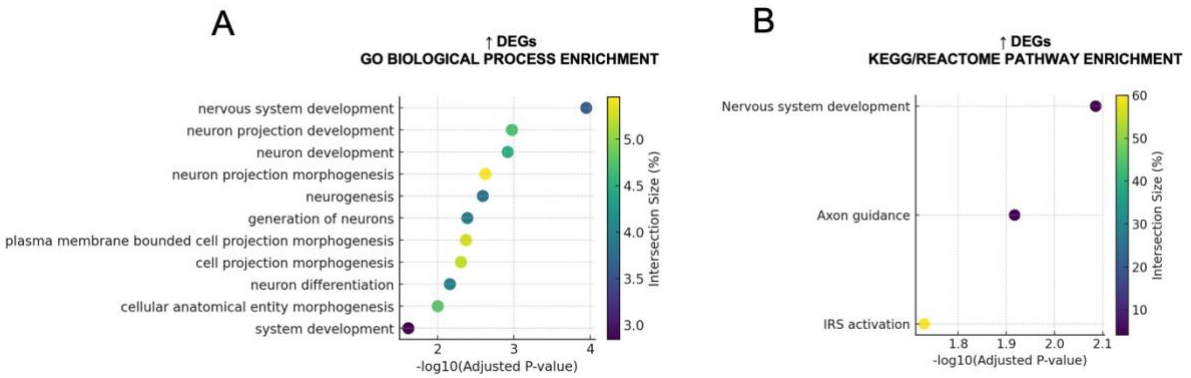

Figure S23. Upregulated DEGs in *FBXO2* KD neurons identify biological pathways in nervous system development and cellular morphogenesis. Pathway enrichment analysis of upregulated differentially expressed genes (DEGs) in *FBXO2* KD neurons treated with ACM, compared to control (ScrRNA, ACM) at DIV21. **(A)** Dot plot of enriched GO terms for upregulated DEGs. The significance of the enrichment is represented as the log10 of the adjusted P-value (x-axis), while y-axis lists enriched biological processes; dot color indicates the percentage of overlapping DEGs for each term. **(B)** Dot plot of enriched KEGG and Reactome pathways, with formatting as in **(A)**.

A

Effect from *FBXO2* KD

ScrRNA vs *FBXO2* KD Number of significant DEGs (filtered by p-value < 0.05, no logFC cutoff)		NM	ACM
DIV14	Downregulated	11	#
	Upregulated	15	#
DIV21	Downregulated	11	333
	Upregulated	46	326
DIV28	Downregulated	5*	2
	Upregulated	18*	7

DIV14 neurons have not been treated with ACM
* LogFC < 0.002

Table reports DEGs, without inclusion of novel transcripts and pseudogenes

B

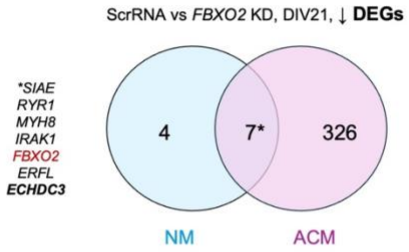

C

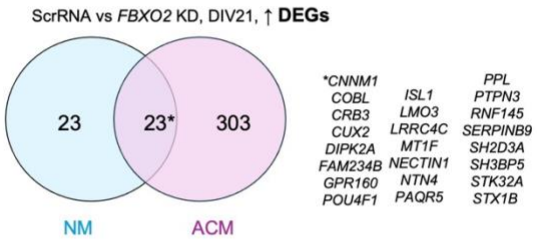

D

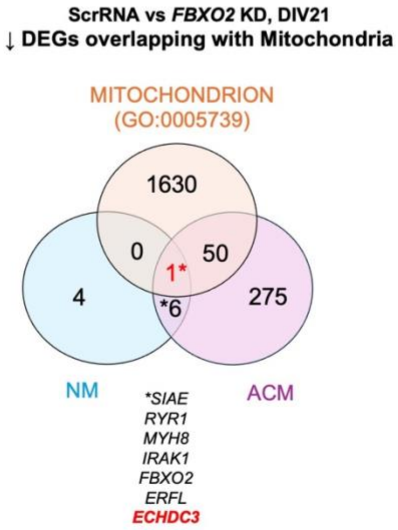

E

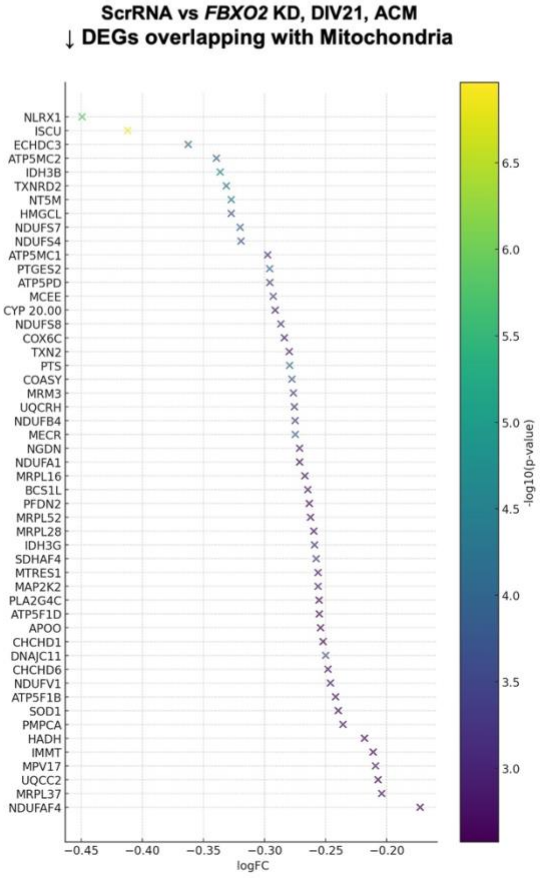

Figure S24. **Transcriptomic profiling of *FBXO2* knockdown neurons identifies gene expression changes in NM and ACM-treatment conditions. (A)** Summary table of the number of significant DEGs (adjusted p-value < 0.05) between ScrRNA and *FBXO2* knockdown neurons across three explored time points (DIV14, 21 and 28), under NM- and ACM-medium change regimes. The count of downregulated and upregulated DEGs is displayed for each condition. DIV14 ACM data are lacking due to ACM treatment regime starting at this time point. DEG counts for NM at DIV28 are marked with an asterisk (*), indicating small but significant log fold-change values (< ±0.002 for both upregulated and downregulated genes, adjusted p-value < 0.05). **(B,C)** Venn diagrams of downregulated (B) and upregulated (C) DEGs upon *FBXO2* knockdown in NM and ACM conditions at DIV21. Shared DEGs are listed alongside. **(D)** Venn diagram highlighting the overlap of downregulated DEGs at DIV21 with mitochondrial genes (GO:0005739) under NM and ACM treatment. Fiftyone genes overlap with mitochondrial terms in ACM-treated *FBXO2* knockdown neurons, while only one gene overlaps for the NM condition. ECHDC3, highlighted in red, is the only gene shared between NM, ACM, and mitochondria groups. **(E)** Scatter plot displaying the log fold-change and -log10 of adjusted P-value for the 51 mitochondria-related downregulated DEGs (Y-axis) in ACM-treated *FBXO2* knockdown neurons at DIV21.

A

Effect from medium change regime

NM vs ACM treatment Number of significant DEGs (filtered by p-value < 0.05, no logFC cutoff)		ScrRNA	FBXO2
DIV21	Downregulated	1082	97*
	Upregulated	1219	356
DIV28	Downregulated	1291	1495
	Upregulated	1355	1551

** Unconclusive pathway enrichment analysis*

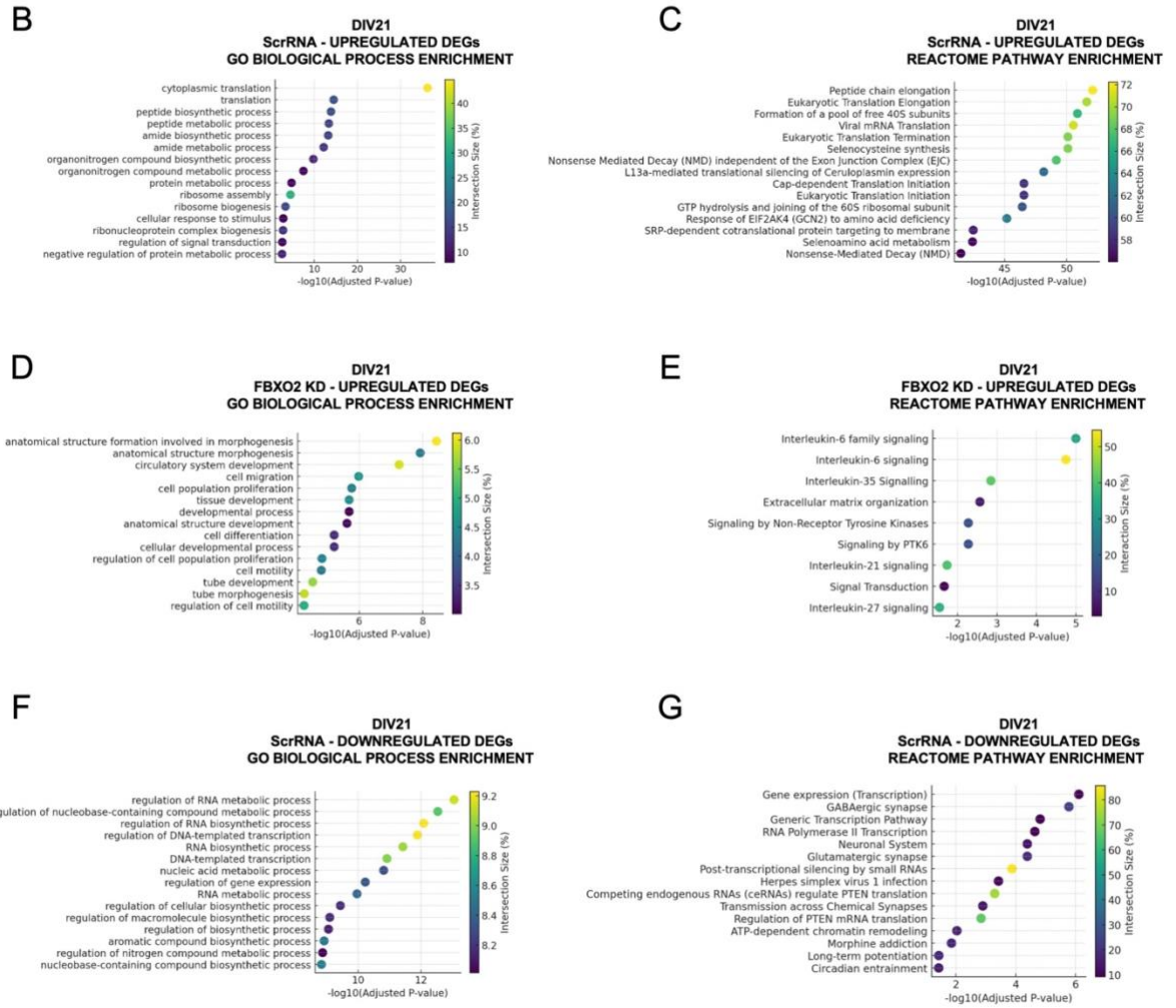

Figure S25. **ACM treatment induces transcriptomic signatures of enhanced cytokine signalling in *FBXO2* knockdown neurons and protein synthesis in ScrRNA neurons. (A)** Summary table displaying the number of significant DEGs (adjusted p-value < 0.05) between NM and ACM-treated ScrRNA or *FBXO2* knockdown neurons at DIV21 and DIV28. Downregulated and upregulated DEG counts are shown for each pairwise comparison. **(B, C)** Results of GO biological process **(B)** and Reactome pathway **(C)** enrichment analysis for upregulated DEGs in ScrRNA neurons treated with ACM vs NM at DIV21. X-axis of each dot plot represents the -log10 of the adjusted P-value, with higher values indicating greater enrichment significance. Dot color represent the intersection size

percentage, indicative of the proportion of significant DEGs associated with each term. **(D, E)** Results of GO biological process **(D)** and Reactome pathway **(E)** enrichment analysis for upregulated DEGs in FBXO2 knockdown neurons at DIV21: Dot plot formatting is as in panels **(B, C)**. **(F, G)** Results of GO biological process **(F)** and Reactome pathway **(G)** enrichment analysis for downregulated DEGs in ScrRNA neurons at DIV21: Dot plot format is consistent with previous panels. Pathway enrichment analysis for FBXO2 knockdown downregulated DEGs at DIV21 was inconclusive (indicated by * in table of panel A).

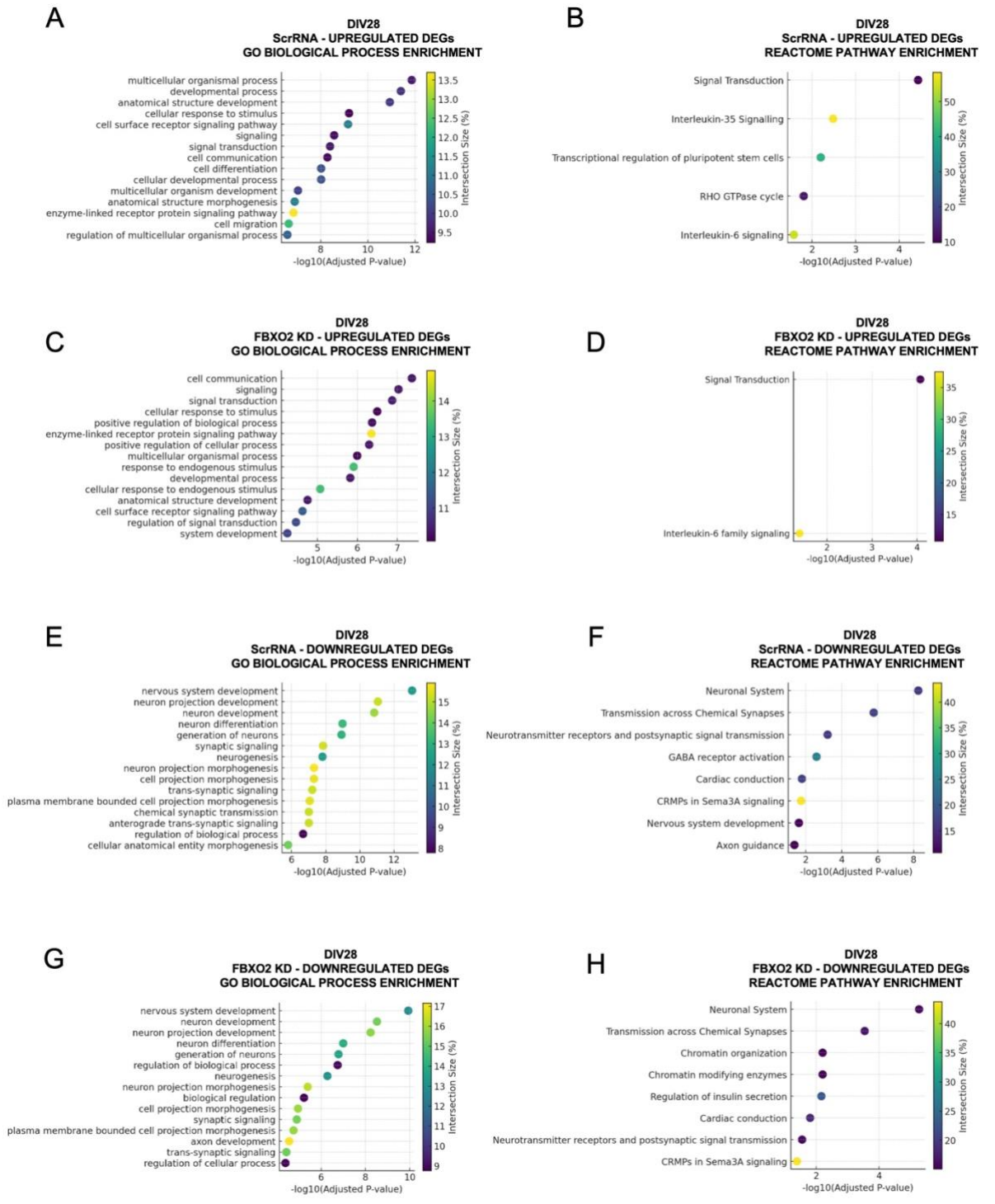

Figure S26. **ACM treatment induces similar pathway enrichment profiles in ScrRNA and *FBXO2* knockdown neurons at DIV28. (A,B)** GO biological process (A) and Reactome pathway (B) enrichment analysis for upregulated DEGs in ScrRNA neurons at DIV28. **(C,D)** GO biological process (C) and Reactome pathway (D) enrichment analysis for upregulated DEGs in *FBXO2* knockdown neurons at DIV28. **(E,F)** GO biological process (E) and Reactome pathway (F) enrichment analysis results for downregulated DEGs in ScrRNA neurons at DIV28. **(G,H)**. GO Biological process (G) and Reactome pathway (H) enrichment analysis results for downregulated DEGs in FBXO2 knockdown neurons at DIV28. Dot plots show -log10 of adjusted P-values on the X-axis, with dot color indicating the intersection size.

Supplementary References

1. Shi Y, Kirwan P, Livesey FJ. Directed differentiation of human pluripotent stem cells to cerebral cortex neurons and neural networks. *Nat Protoc* 2012; **7**(10)**:** 1836-1846.
2. Wang C, Najm R, Xu Q, Jeong D-e, Walker D, Balestra ME *et al.* Gain of toxic apolipoprotein E4 effects in human iPSC-derived neurons is ameliorated by a small-molecule structure corrector. *Nat Med* 2018; **24**(5)**:** 647-657.